

**METEOROLOGICAL AND AIR QUALITY IMPACTS
OF HEAT ISLAND MITIGATION MEASURES
IN THREE U.S. CITIES**

Haider Taha, Sheng-chieh Chang, and Hashem Akbari
Heat Island Group
Environmental Energy Technologies Division
Lawrence Berkeley National Laboratory
Berkeley, CA 94720

April 2000

This work was supported by the U.S. Environmental Protection Agency (USEPA) under IAG No. DW89938442-01-2 and by the Assistant Secretary for Energy Efficiency and Renewable Energy, Building Technologies, of the U.S. Department of Energy under Contract No. DE-AC03-76SF00098.

ACKNOWLEDGEMENTS

The study was sponsored by the USEPA under the Heat Island Reduction Initiative (HIRI)/Urban Heat Island Pilot Project (UHIPP), Virginia Gorsevski, Project Manager. We acknowledge support, guidance, and assistance from Virginia Gorsevski and Jeanne Briskin, Climate Protection Division, USEPA, Washington, DC. We would like to thank the following individuals for providing data for use in this modeling effort: 1) Elliot Mulberg at the California Air Resources Board, 2) John Babin at the Louisiana Department of Environmental Quality), and 3) Patrick Barickman at the Utah Division of Air Quality. We acknowledge the MCNC for providing the PAVE software for free use in visualizing the input to and output from the Urban Airshed Model.

Note on units

This report is written using SI units. To make it easier for readership, British system units are also given in parentheses.

ABSTRACT

This report investigates the air pollution reduction benefits associated with mitigating urban heat islands in three U.S. cities. The effects of these measures in Salt Lake City, Baton Rouge, and Sacramento were evaluated through mesoscale meteorological and air quality modeling. The simulations indicate that for these three U.S. cities, adopting heat island reduction measures can result in various meteorological and air quality changes. The meteorological simulations suggest that each of the three pilot cities benefits from reduced ambient air temperatures. Decreases typically range from 1 to 2K (1.8 - 3.6°F) over modified areas.

In Salt Lake City, reductions in ambient air temperatures reach up to 2K (3.6°F) at 1600 LST. The city achieves reductions in ozone concentrations of up to 3 or 4 ppb, the equivalent of about 3.5% if it were compared to an urban peak of 95 ppb. In Baton Rouge, reductions in ambient air temperatures of 0.75K (1.4°F) are possible and ozone reductions reach up to 4 or 5 ppb, the equivalent of about 4% if compared to an urban peak of 113 ppb. Finally, Sacramento enjoys reductions of 1.2K (2.2°F) as a result of heat island mitigation measures. Although these temperature reductions are not as large as those experienced in Salt Lake City, for example, their impacts on ozone are relatively larger, with reductions of up to 10 ppb from peak ozone concentrations (about 7% of the peak of 139 ppb). Sacramento enjoys larger reductions in ozone as a result of its larger geographical area.

The modeling work shows that each of the three regions discussed in this report can benefit from implementing heat island mitigation measures. Clearly, the extent to which urban areas can effectively improve local air quality through heat island mitigation depends on numerous factors. These include meteorology and climate, geography, scale, topography, basin morphology, proximity to water bodies, land-use patterns, precursor emission rates and mix, baseline albedo and vegetative fraction distributions, and potential for modification (increase in albedo and vegetative fraction). Based on our modeling efforts, we found that the larger the modified area, the larger the impacts on meteorology and air quality.

TABLE OF CONTENTS

Acknowledgements	ii
Abstract	iii
Table of Contents	v
List of Abbreviations	vii
List of Figures	viii
List of Tables	x
Executive Summary	1
Background	1
Meteorological impacts	2
Ozone Concentrations Implications	2
Summary of Results	3
Conclusions	4
Introduction	5
The Urban Heat Island Effect	5
Objective and Organization of the Report	5
1. Modeling method	5
1.A Overview	5
1.B Meteorological modeling	7
1.B.1 Models and episodes	7
1.B.2 Assumptions	8
Surface characterization	8
Salt Lake City UT	13
Baton Rouge LA	14
Sacramento CA	15
Surface change scenarios	16
1.B.3 Initial and Boundary Conditions	18
Initial conditions	19
Lateral boundary conditions	19
Top boundary conditions	19
Lower boundary conditions	20
1.C Photochemical modeling	20
1.C.1 Models and Data	20
1.C.2 Approach	22
Emission Inventories	22
Air Quality Initial and Boundary Conditions	22
Four Dimensional Mapping	22
Temperature	23
Mixing Height	23
Wind	23

Specific Humidity	24
Anthropogenic Precursor Emissions	24
Biogenic VOC Emissions	24
Mapping Changes in Initial and Boundary Conditions	25
Modeling Domains and Episodes	25
2. Modeling Results	26
2.A Meteorological Modeling Results	26
Overview	26
Salt Lake City, Utah	26
Base Case Conditions	26
Modified Scenario	26
Baton Rouge, Louisiana	28
Base Case Conditions	28
Modified Scenario	29
Sacramento, California	30
Base Case Conditions	30
Modified Scenario	31
Summary of Meteorological Modeling Results	32
2.B Air Quality Modeling Results	34
Overview	34
Salt Lake City, Utah	35
Base Case Conditions	35
Modified Scenario	36
Baton Rouge, Louisiana	37
Base Case Conditions	37
Modified Scenario	38
Sacramento, California	40
Base Case Conditions	40
Modified Scenario	40
Summary of Photochemical Modeling Results	42
Emission Equivalents of IAIV Strategies	44
3. Conclusion	45
Summary	45
Caveats	46
Issues with selection of cities	47
Issues with the modeling process	47
Issues with input data	48
Issues with surface-modification scenarios assumptions	48
4. References	49

LIST OF ABBREVIATIONS

AGL	Above ground level
BR	Baton Rouge, Louisiana
BVOC	Biogenic volatile organic compounds
CSUMM	Colorado State University Mesoscale Model
DEM	Digital Elevation Model
IAIV	Increased albedo/Increased vegetation
LULC	Land use/Land cover
MSL	Mean sea level
NO _x	Oxides of nitrogen
SAC	Sacramento, California
SIP	State Implementation Plan
SLC	Sale Lake City, Utah
SST	Sea-surface temperature
PAN	Peroxyacetylnitrate
UAM	Urban airshed model
UAM-V	Urban airshed model (variable-grid version)
UHI	Urban heat island
UHIPP	Urban heat island pilot project
USGS	United States Geological Survey
VOC	Volatile organic compounds

LIST OF FIGURES

M1	Modeling flow chart
M2	Parameter modeling bubble diagram
SLC-1	Salt Lake City (SLC) region's topography
SLC-2	Gridded albedo for the SLC domain
SLC-3	Gridded vegetative fraction for the SLC domain
SLC-4	Gridded density for the SLC domain
SLC-5	Gridded thermal diffusivity for the SLC domain
SLC-6	Gridded surface wetness for the SLC domain
SLC-7	Gridded roughness length for the SLC domain
SLC-8	Gridded specific heat for the SLC domain
SLC-9	Gridded maximum anthropogenic heat flux for the SLC domain
SLC-10	Increased albedo in the SLC domain
SLC-11	Increased vegetation in the SLC domain
SLC-12	Base-case air temperature in the SLC domain
SLC-13	Base-case wind field for the SLC domain
SLC-14	Base-case mixing height for the SLC domain
SLC-15	Change in air temperature in the SLC domain resulting from IAIV
SLC-16	IAIV wind field in the SLC domain
SLC-17	IAIV mixing height in the SLC domain
SLC-18	Base-case NO _x emissions at 1400 LST in SLC
SLC-19	Base-case NO _x emissions at 1600 LST in SLC
SLC-20	Base-case isoprene emissions at 1400 LST in SLC
SLC-21	Base-case isoprene emissions at 1600 LST in SLC
SLC-22	Base-case (peak) ozone concentrations in the SLC domain
SLC-23	Change in NO _x emissions at 1400 LST in SLC resulting from IAIV
SLC-24	Change in NO _x emissions at 1600 LST in SLC resulting from IAIV
SLC-25	Change in isoprene emissions at 1400 LST in SLC resulting from IAIV
SLC-26	Change in isoprene emissions at 1600 LST in SLC resulting from IAIV
SLC-27	Change in ozone concentrations in the SLC domain resulting from IAIV
BR-1	Baton Rouge (BR) region's topography
BR-2	Gridded albedo for the BR domain
BR-3	Gridded vegetative fraction for the BR domain
BR-4	Gridded density for the BR domain
BR-5	Gridded thermal diffusivity for the BR domain
BR-6	Gridded surface wetness for the BR domain
BR-7	Gridded roughness length for the BR domain
BR-8	Gridded specific heat for the BR domain
BR-9	Gridded maximum anthropogenic heat flux for the BR domain
BR-10	Increased albedo in the BR domain
BR-11	Increased vegetation in the BR domain
BR-12	Base-case air temperature in the BR domain

BR-13 Base-case wind field for the BR domain
 BR-14 Base-case mixing height for the BR domain
 BR-15 Change in air temperature in the BR domain resulting from IAIV
 BR-16 IAIV wind field in the BR domain
 BR-17 IAIV mixing height in the BR domain
 BR-18 Base-case NO_x emissions at 1400 LST in BR
 BR-19 Base-case NO_x emissions at 1600 LST in BR
 BR-20 Base-case isoprene emissions at 1400 LST in BR
 BR-21 Base-case isoprene emissions at 1600 LST in BR
 BR-22 Base-case (peak) ozone concentrations in the BR domain
 BR-23 Change in NO_x emissions at 1400 LST in BR resulting from IAIV
 BR-24 Change in NO_x emissions at 1600 LST in BR resulting from IAIV
 BR-25 Change in isoprene emissions at 1400 LST in BR resulting from IAIV
 BR-26 Change in isoprene emissions at 1600 LST in BR resulting from IAIV
 BR-27 Change in ozone concentrations in the BR domain resulting from IAIV

SAC-1 Sacramento (SAC) region's topography
 SAC-2 Gridded albedo for the SAC domain
 SAC-3 Gridded vegetative fraction for the SAC domain
 SAC-4 Gridded density for the SAC domain
 SAC-5 Gridded thermal diffusivity for the SAC domain
 SAC-6 Gridded surface wetness for the SAC domain
 SAC-7 Gridded roughness length for the SAC domain
 SAC-8 Gridded specific heat for the SAC domain
 SAC-9 Gridded maximum anthropogenic heat flux for the SAC domain
 SAC-10 Increased albedo in the SAC domain
 SAC-11 Increased vegetation in the SAC domain
 SAC-12 Base-case air temperature in the SAC domain
 SAC-13 Base-case wind field for the SAC domain
 SAC-14 Base-case mixing height for the SAC domain
 SAC-15 Change in air temperature in the SAC domain resulting from IAIV
 SAC-16 IAIV wind field in the SAC domain
 SAC-17 IAIV mixing height in the SAC domain
 SAC-18 Base-case NO_x emissions at 1400 LST in SAC
 SAC-19 Base-case NO_x emissions at 1600 LST in SAC
 SAC-20 Base-case isoprene emissions at 1400 LST in SAC
 SAC-21 Base-case isoprene emissions at 1600 LST in SAC
 SAC-22 Base-case (peak) ozone concentrations in the SAC domain
 SAC-23 Change in NO_x emissions at 1400 LST in SAC resulting from IAIV
 SAC-24 Change in NO_x emissions at 1600 LST in SAC resulting from IAIV
 SAC-25 Change in isoprene emissions at 1400 LST in SAC resulting from IAIV
 SAC-26 Change in isoprene emissions at 1600 LST in SAC resulting from IAIV
 SAC-27 Change in ozone concentrations in the SAC domain resulting from IAIV
 SAC-28 Peak ozone isopleths for July 13 at 1700 LST in Sacramento

LIST OF TABLES

Table 1	Assumed thermophysical properties of LULC	10
Table 2	Sacramento surface makeup	11
Table 3	Assumed properties for 30-cm resolution data	12
Table 4	Update thermophysical properties of LULC	12
Table 5	Some aspects of the modeling domains	16
Table 6	IAIV scenarios assumptions	17
Table 7	Albedo and vegetative fraction changes statistics	18
Table 8	Modeling domains and grids	25
Table 9	Summary of urban air temperature and modifications	33
Table 10	Domain-averaged mixing height and changes	33
Table 11	Some aspects of simulated wind fields and changes	34
Table 12	Peak ozone concentrations and changes	42
Table 13	Ozone concentration changes	42
Table 14	Largest ozone concentration changes	43
Table 15	D/I ratio at selected hours	43
Table 16	Temperature-sensitivity for ozone concentration changes	43

EXECUTIVE SUMMARY

This report investigates the air pollution reduction benefits associated with mitigating urban heat islands in three U.S. cities. The Urban Heat Island Pilot Project (UHIPP) conducted a study to quantify the impacts of increased albedo of urban surfaces and urban reforestation on ozone air quality, using mesoscale meteorological and photochemical models. The effects of these measures in Salt Lake City, Baton Rouge, and Sacramento were evaluated. The simulations indicate that for these three U.S. cities, adopting heat island reduction measures can result in various meteorological and air quality changes. Overall, there is improvement in ozone air quality. One city also experienced reductions in peak ozone concentrations as a result of these measures. Average temperature reductions due to heat island mitigation in the three pilot cities ranged up to 2K (3.6 °F) over modified areas. Corresponding ozone reductions ranged from 1 to 8.3 ppb/K (0.6-4.6 ppb/°F).

Background

Modeling and field studies suggest that heat island reduction strategies can reduce surface and air temperatures. The general impacts on air quality and energy use of relatively lower ambient temperatures include: 1) a reduction in temperature-dependent photochemical reaction rates; 2) a decrease in temperature-dependent biogenic hydrocarbon emissions; 3) a decrease in evaporative losses of organic compounds from mobile and stationary sources; and 4) a decreased need for cooling energy, generating capacity, and, ultimately, emissions from power plants. Thus, increasing urban surface reflectivity, or “albedo”, and the amount of vegetation in urban areas, has the potential to reduce ozone formation.

Recent field-measurements and modeling studies support these conclusions. For example, Gabersek and Taha (1996) and Taha (1996,1997) show that implementing heat island reduction strategies may be an effective way of reducing urban air temperatures by up to 5K (9°F) in summer, reducing exceedance exposure to ozone by 10-20%. On the other hand, Akbari et al. (1997a,b), Parker and Barkaszi (1997), Simpson and McPherson (1997), show that potential savings in cooling energy use, due to increased albedo of building and urban surfaces and urban reforestation, can also be quite significant. As with previous studies, the UHIPP attempts to quantify the impacts of heat island mitigation measures on energy use, meteorology, and air quality. However, this study uses, to the extent that it is possible, input that was obtained directly from appropriate environmental agencies in each of the pilot cities, in order to ensure the applicability of these data. In this study, more realistic modeling approaches were followed and more innovative surface characterization (aerial urban fabric analysis) was performed, than in previous studies.

Meteorological Impacts

Meteorological simulations were performed for the base case (current conditions), and for several modified scenarios for each region (which assume adoption of heat island reduction measures). The output from meteorological models was used as input to photochemical models (directly) and to emission processors (indirectly). This allowed for adjustment in the emissions of various precursors (such as NO_x and VOC) to changes in meteorological conditions.

In this executive summary, we look briefly at air temperature (since it is relevant to both energy use and meteorology/air quality), but the report discusses all meteorological variables and changes therein. Table EX.1 is a sample temperature reduction resulting from heat island reduction measures in each of the three pilot cities for selected hours. It shows the base case temperature and the cooling resulting from heat island reduction. The temperature shown is representative of the urban area (e.g., city center) in each of the three regions and is for the last day of the respective episodes. The last day is selected to ensure that the effects of initial conditions and model spin-up are minimal.

Table EX.1: Air temperatures and reductions at 0600 and 1600 local standard time (LST) for each of the three pilot cities.

Region		0600 LST	1600 LST
Salt Lake City	Base case temperature	293K (68°F)	305K (89.6°F)
	Change in temperature from heat island reduction strategies	-1K (-1.8°F)	-2K (-3.6°F)
Baton Rouge	Base case temperature	293K (68°F)	307K (93.2°F)
	Change in temperature from heat island reduction strategies	0	-0.75K (-1.4°F)
Sacramento	Base case temperature	300K (80.6°F)	311K (100.4°F)
	Change in temperature from heat island reduction strategies	-1K (-1.8°F)	-1.2K (-2.2°F)

The simulations suggest that all of the cities enjoy greater reductions in air temperature in the afternoon than in the morning. Salt Lake City enjoys the largest reductions in air temperature as a result of heat island reduction strategies, followed by Sacramento, and then Baton Rouge. This is due to the fact that in Salt Lake City, the level of modification in albedo and vegetation was slightly higher than in the other two cities.

Ozone Concentrations Implications

Photochemical simulations in this study were performed using various versions of the Urban Airshed Model (UAM) to determine the impact of heat island mitigation strategies on ozone air quality. The UAM is a three-dimensional, Eulerian, photochemical model that simulates the advection, diffusion, transformation, emission, and deposition of

pollutants. The UAM accounts for emissions from area and point sources, elevated stacks, mobile and stationary sources, and vegetation (biogenic emissions). The model has been approved and recommended by the US EPA for ozone air quality studies of urban areas (EPA 1986).

The results of the photochemical modeling indicate that all three regions experience improvements in air quality through reductions in ozone levels during the day as a result of adopting heat island reduction measures. However, only Sacramento experiences significant reductions in peak ozone concentrations (i.e., the domain peak). This is possibly due to the fact that Sacramento covers a larger geographical area, thus allowing for larger cumulative impacts from heat island control strategies. Table EX.2 is a sample ozone concentration changes for each region.

Table Ex.2 Some air quality modeling result indicators.

1	2		3
Region	Largest decrease in ozone concentrations * (at selected hours)		Change in peak ozone **
Salt Lake City	4 ppb (at 7 a.m.)	3 ppb (at 2 p.m.)	0%
Baton Rouge	5 ppb (at 9 a.m.)	4 ppb (at 12 p.m.)	- 0.8%
Sacramento	7 ppb (at 2 p.m.)	10 ppb (at 4 p.m.)	- 6.5%

*Anywhere in the domain

**At location and time of urban peak (column3 is totally unrelated to column 2)

Summary of Results

While all meteorological fields are affected by changes in surface properties (changes in albedo and vegetative cover), we discussed only temperature in this summary. The meteorological simulations suggest that each of the three pilot cities benefits from reduced ambient air temperatures. Decreases typically range from 1 to 2K (1.8-3.6°F) over modified areas. Reduced ambient air temperatures reduce the overall demand for cooling energy in buildings. While all three cities achieve reductions in ozone concentrations as a result of heat island mitigation, Sacramento enjoys additional benefits from reductions in peak ozone concentrations.

In Salt Lake City, reductions in ambient air temperatures reach up to 2K (3.6°F) at 1600 LST. The city achieves reductions in ozone concentrations by up to 3 or 4 ppb, the equivalent of about 3.5% if it were compared to an urban peak of 95 ppb. In Baton Rouge, reductions in ambient air temperatures of 0.75K (1.4°F) are possible and ozone reductions reach up to 4 or 5 ppb, the equivalent of about 4% if compared to an urban peak of 113 ppb. In Baton Rouge, the temperature decrease results primarily from increased albedo. This is due to the higher surface moisture in the area, which tends to limit evapotranspiration from increased vegetative cover. Finally, Sacramento enjoys reductions of 1.2K (2.2°F) as a result of heat island mitigation measures. Although these

temperature reductions are not as large as those experienced in Salt Lake City, for example, their impacts on ozone concentrations are relatively larger, with reductions of up to 10 ppb from peak ozone concentrations (about 7% of the peak of 139 ppb). Sacramento enjoys larger reductions in ozone as a result of its larger geographical area.

Conclusions

Each of the three regions discussed in this report can benefit from implementing heat island mitigation measures. Clearly, the extent to which urban areas can effectively improve local air quality through heat island mitigation measures depends on numerous factors. These include meteorology and climate, geography, scale, topography, basin morphology, proximity to water bodies, land-use patterns, precursor emission rates and mix, baseline albedo and vegetative fraction distributions, and potential for modification (increasing albedo and vegetative fraction). Based on our modeling efforts, we found that the larger the modified area, the larger the impacts on meteorology and air quality. This is important in large metropolitan areas where peak ambient temperatures can be decreased by as much as 5K (9°F) locally and by up to 3K (5°F) on average, such as in Los Angeles, California. The reduction in ozone concentrations, therefore, can be larger than what has been simulated in these three cities.

INTRODUCTION

In 1997, the U.S. Environmental Protection Agency (EPA) initiated the Urban Heat Island Pilot Project (UHIPP). The UHIPP is an effort to investigate the use of high-albedo roofs and pavements, and increased urban vegetation to improve air quality in urban areas. The regions surrounding the cities of Sacramento CA, Salt Lake City UT, and Baton Rouge LA were selected for the UHIPP and are the subject of this report.

The Urban Heat Island Effect

The heat island effect occurs largely in metropolitan areas where the buildings and paved surfaces tend to absorb incoming solar radiation. The result is to increase ambient air temperatures in urban centers relative to surrounding areas. In many cases, these built-up surfaces have replaced natural vegetation, taking away the additional benefit that vegetation can provide when it lowers ambient air temperatures through the process of evapotranspiration. Urban heat islands can also lead to worsened air quality for two primary reasons. One is the accelerated rate of photochemical ozone production at higher temperatures and the other is the increase in temperature-sensitive emissions of ozone precursors.

Strategies to reduce urban heat islands include increasing the albedo of built-up surfaces and increased vegetative cover. These measures can reduce ambient air temperature and slow down smog formation. As a result, communities and cities that choose to implement these cost-effective heat island reduction strategies can benefit from reduced levels of smog and improvements in the overall health and productivity of the community.

Objective and Organization of the Report

This report summarizes recent efforts to model the impacts of large-scale changes in the urban environment by increasing the albedo of urban surfaces and urban reforestation. Section One of this report describes the modeling method that were used to perform the analysis. Section Two discusses the results of the analysis in terms of overall meteorology and ozone changes for each of the three pilot cities. Finally, Section Three of this report summarizes key observations and conclusions.

1. Modeling Method

1. A Overview

Several steps were taken to perform the meteorological and photochemical simulations for this study. First, the modeling domains were characterized in terms of surface

properties, land use/land cover (LULC), topography, and water/land distributions. These were based on data obtained from the United States Geological survey (USGS), remotely-sensed information, aerial photographs, and in-situ field campaigns, where applicable. In terms of surface characterization, several parameters were quantified. These are needed to specify the lower boundary (surface) in the meteorological and air quality models. Parameters needed by these models include, but are not limited to, density, specific heat, albedo, normalized difference vegetation index (NDVI), thermal inertia, anthropogenic heat flux, thermal diffusivity, moisture content, and roughness length. All these parameters were gridded at a resolution corresponding to that of the simulations for each region. In addition, all of these parameters were computed and re-specified for each modification scenario, e.g., changes in albedo and urban vegetation fraction. These changes were then re-mapped onto the domain's grid accordingly.

The domains characterization in terms of meteorological initial and boundary conditions was then undertaken. Initial conditions were based on observational data representing the times and episodes of interest. Following this step, emission input data were prepared for use in the photochemical model (e.g., UAM). In this study, the emission information and pollutant-concentration boundary conditions were obtained from the state air quality regulatory agencies in each region. These include emission rates for all relevant pollutants and chemical species from area, point, mobile, and biogenic sources.

The next step was the initiation of meteorological modeling of the selected domains for the specified episodes. The episodes correspond to those used by the cities in their SIP attainment demonstration modeling. Typically, these are hot summer episodes of poor air quality such as late May to mid-August, although in some cases the modeling episodes may not capture the worst air quality conditions experienced in the regions. The meteorological simulations were performed for up to four days at a time for the base-case conditions as well as the modified scenarios. The meteorological simulations were performed off-line with respect to air quality models. Results from these simulations were used as direct boundary condition input to photochemical models (temperature, wind, mixing height, specific humidity) as well as input to emission processors (indirectly) to adjust the emissions of various precursors to changes in meteorological conditions. The changes in meteorology and emissions from all affected sources were then mapped onto the input to UAM. This modified input was used to simulate the effects and impacts of IAIV strategies (Increased Albedo, Increased Vegetation) in each region, accordingly.

To summarize, the following tasks were performed for this study:

1. Obtain and derive meteorological, surface characteristics, and air quality data;
2. Characterize urban surfaces through analysis of aerial photographs, remotely-sensed data, and information from local cities and state agencies;
3. Define base and modified scenarios for simulations;

4. Perform meteorological simulations for base and modified scenarios;
5. Perform air-quality simulations for base and modified scenarios;
6. Analyze the simulation results to quantify the potential role of heat island mitigation measures in reducing smog production; and
7. Extrapolate the meteorological simulation results to modify typical weather data used in modeling annual building energy use in each region.

In this section, we describe both the meteorological and photochemical modeling methods undertaken in this study, including the assumptions (i.e. surface modifications) used to model the impacts of heat island mitigation measures in each of the three regions. The flowcharts shown in Figures M1 and M2 help explain some aspects of the modeling method.

[Figure M1 is self-explanatory, while the entries in Figure M2 are as follows: a is albedo, K is solar radiation, T_s and T_a are surface and air temperatures, respectively, LE is latent heat flux, L is long-wave radiative flux, β is Bowen Ratio, Z_o is roughness length, D is dry deposition, $u, v,$ and $w,$ are the 3-dimensional components of the wind vector, TKE is turbulent kinetic energy, Z_i is mixing height, C_5H_8 is isoprene, and $C_{10}H_{16}$ are monoterpenes]

1.B Meteorological Modeling

1.B.1 MODELS AND EPISODES

The meteorological simulations were performed with an LBNL-modified version of the Colorado State University Mesoscale Model (CSUMM). The LBNL modifications to CSUMM are described in Taha (1999,1997,1996). The CSUMM is a hydrostatic, primitive-equation, three-dimensional Eulerian model originally developed by Pielke (1974). The model is incompressible, and employs a σ_z coordinate system. It uses a first order closure scheme in treating sub-grid scale terms of the governing differential equations. The model's domain in this study is set to 9 km high with an underlying soil layer that is 50 cm deep. The CSUMM generates three-dimensional fields of prognostic variables as well as a mixing-height field that can be used as input to air quality models, such as the UAM. For a description of CSUMM, see Kessler and Douglas (1992).

CSUMM's performance in *this* type of applications has been evaluated in the past, e.g., Taha (1996,1997), and found to be reasonable. Problems with the mixing height computation were identified, but Taha's work for Atlanta and Los Angeles concluded that the model performance was acceptable based on model benchmark tests, e.g., Pielke (1984). The purpose of this study was not necessarily to reproduce observed meteorological conditions hour by hour; rather, it was to look at the sensitivity of some parameters as a result of changes in surface properties during representative summer days as appropriate for each region. For this type of application, the CSUMM is a reasonable

tool, especially for cloud-free episodes. In addition, a semi-quantitative evaluation of model performance for base-case simulations was performed in this study. In general, the model was found to perform relatively well, although some concerns were raised.

The meteorological modeling episodes simulated in this study correspond closely to those used in State Implementation Plan (SIP) attainment demonstration modeling. For photochemical modeling, the SIP episodes for Salt Lake City, Baton Rouge, and Sacramento, are August 11-12 (1996), May 24-25 (1990), and July 11-13 (1990), respectively. The meteorological simulation episodes in this study were one day longer than the corresponding SIP episodes to allow for model spin up and adjustment. Thus, the meteorological simulations were performed for up to four days at a time for each domain. In general, the photochemical modeling episodes are selected by the states and cities to represent summer ozone conditions, but some of these episodes may not capture the worst-case scenarios, e.g., high-ozone periods in the regions. Because of this and model-specific issues, the UAM simulations can underpredict some of the high ozone concentrations observed in these three regions.

1.B.2 ASSUMPTIONS

Surface Characterization

In order to perform the meteorological modeling of the base-case (current) conditions in each region, partial input of gridded surface physical properties was derived based on USGS data. Two types of USGS data were used: the Digital Elevation Model (DEM) and the Land Use and Land Cover (LULC) digital data, which provide information on nine major classes of land use with several subcategories each. The resolution of these data is 200 m, arranged in arrays conforming to the Universal Transverse Mercator (UTM) projection. The standard USGS categories and subcategories of LULC (used in this study to characterize the surface) include:

1 Urban or Built-Up Land

- 11 Residential
- 12 Commercial/Services
- 13 Industrial
- 14 Transportation, Communications
- 15 Industrial and Commercial
- 16 Mixed Urban or Built-Up Land
- 17 Other Urban or Built-Up Land

2 Agricultural Land

- 21 Crop land and Pasture
- 22 Orchards, Groves, Vineyards, Nurseries
- 23 Confined Feeding Operations
- 24 Other Agricultural Land

3 Rangeland

- 31 Herbaceous Rangeland
- 32 Shrub and Brush Rangeland

	33 Mixed Rangeland
4 Forest Land	41 Deciduous Forest Land
	42 Evergreen Forest Land
	43 Mixed Forest Land
5 Water	51 Streams and Canals
	52 Lakes
	53 Reservoirs
	54 Bays and Estuaries
6 Wetland	61 Forested Wetlands
	62 Nonforested Wetlands
7 Barren Land	71 Dry Salt Flats
	72 Beaches
	73 Sandy Areas Other than Beaches
	74 Bare Exposed Rock
	75 Strip Mines, Quarries, and Gravel Pits
	76 Transitional Areas
	77 Mixed Barren Land
8 Tundra	81 Shrub and Brush Tundra
	82 Herbaceous Tundra
	83 Bare Ground
	84 Wet Tundra
	85 Mixed Tundra
9 Perennial Snow or Ice	91 Perennial Snowfields
	92 Glaciers

This table lists the categories that form the basis of the LULC classification system; it does not imply that all categories were present in the modeling domains defined for this project. For this study, each of these LULCs is assigned a set of thermophysical property values based on empirical or published data, e.g., Pielke (1984), as well as our own experience and field observations. Table 1, shows the values assumed for each LULC. In this table, α is albedo, Z_0 is roughness length (cm), η is surface wetness (volumetric ratio of water to soil), ρ is density (g cm^{-3}), k is thermal diffusivity (cm^2s^{-1}), c is specific heat ($\text{Jg}^{-1}\text{K}^{-1}$), Q_f is maximum anthropogenic heat flux (W m^{-2}) for corresponding LULC, and f is vegetation fraction. Of the urban categories, 11 is residential, 12 is commercial, 13 is industrial, 14 is transportation/communication, 15 is industrial/commerce, 16 is mixed urban/built-up land, and 17 is other urban/built up, as defined in the table above.

Table 1: Assumed Thermophysical Properties of Land-Use Categories

<i>USGS LULC</i>	α	Z_0 (cm)	η	ρ (g cm ⁻³)	k (cm ² s ⁻¹)	C (J g ⁻¹ K ⁻¹)	Q_f (W m ⁻²)	f
Urban								
11	0.16	35	0.05	1.6	0.0033	0.30	10.0	0.20
12	0.14	150	0.05	1.6	0.0033	0.30	10.0	0.05
13	0.20	35	0.05	1.6	0.0033	0.30	10.0	0.05
14	0.16	35	0.05	1.6	0.0033	0.30	40.0	0.05
15	0.14	35	0.05	1.6	0.0033	0.30	40.0	0.05
16	0.16	35	0.05	1.6	0.0033	0.30	10.0	0.05
17	0.14	35	0.05	1.6	0.0033	0.30	10.0	0.05
Agricultural								
21	0.18	12	0.30	1.8	0.0038	0.44	0.0	0.60
22	0.16	12	0.30	1.8	0.0038	0.44	0.0	0.60
23	0.12	12	0.30	1.8	0.0038	0.44	0.0	0.60
24	0.15	12	0.30	1.8	0.0038	0.44	0.0	0.60
Range								
31	0.18	5	0.03	1.6	0.0050	0.30	0.0	0.10
32	0.18	5	0.03	1.6	0.0050	0.30	0.0	0.10
33	0.18	5	0.03	1.6	0.0050	0.30	0.0	0.10
Forest								
41	0.15	350	0.20	1.8	0.0057	0.35	0.0	0.50
42	0.18	350	0.20	1.8	0.0057	0.35	0.0	0.50
43	0.16	350	0.20	1.8	0.0057	0.35	0.0	0.50
Water								
51	0.08	1	1.00	1.0	0.0015	1.00	0.0	0.0
52	0.06	1	1.00	1.0	0.0015	1.00	0.0	0.0
53	0.08	1	1.00	1.0	0.0015	1.00	0.0	0.0
54	0.06	1	1.00	1.0	0.0015	1.00	0.0	0.0
Wetland								
61	0.16	0.001	0.50	1.5	0.0020	0.80	0.0	0.25
62	0.16	0.001	0.50	1.5	0.0020	0.80	0.0	0.25
Barren land								
71	0.40	0.05	0.01	1.6	0.0050	0.30	0.0	0.0
72	0.40	0.05	0.01	1.6	0.0050	0.30	0.0	0.0
73	0.30	0.05	0.01	1.6	0.0050	0.30	0.0	0.0
74	0.30	0.05	0.01	1.6	0.0050	0.30	0.0	0.0
75	0.25	0.05	0.01	1.6	0.0050	0.30	0.0	0.0
76	0.18	0.05	0.01	1.6	0.0050	0.30	0.0	0.0
77	0.18	0.05	0.01	1.6	0.0050	0.30	0.0	0.0
Tundra								
81	0.18	10	0.05	1.3	0.0038	0.35	0.0	0.20
82	0.18	10	0.05	1.3	0.0038	0.35	0.0	0.20
83	0.16	10	0.05	1.3	0.0038	0.35	0.0	0.20
84	0.20	10	0.05	1.3	0.0038	0.35	0.0	0.20
85	0.19	10	0.05	1.3	0.0038	0.35	0.0	0.20
Ice								
91	0.80	0.005	0.20	0.8	0.0100	0.21	0.0	0.0
92	0.35	0.005	0.20	0.8	0.0100	0.21	0.0	0.0

Although the assumed thermophysical properties of land-use categories listed above are both reasonable and comparable to observational values (where available), we made an attempt to augment portions of this information by performing a more detailed analysis of the pilot regions. This was done by using aerial-photography mapping to develop a fine-resolution (30 cm) characterization of the surface and obtain accurate location-specific gridded values of relevant parameters needed in developing part of the input to meteorological models. As of this report's writing, orthophotos have been obtained for two of the three pilot cities — Sacramento and Salt Lake City.

In summer of 1998, we sub-contracted a private aerial photography company to fly over Sacramento, CA and obtain orthophotos from various sub-regions. The sub-regions were selected by us to represent a wide range of LULCs found in the Sacramento area and its suburbs. Flights over Salt Lake City were completed in summer 1999 and the data analysis is underway. The land uses and covers we identified in the orthophotos were then characterized and mapped onto appropriate USGS LULCs to establish a basis for extrapolation to other areas. Analysis of data from the Sacramento flights provided a wealth of information regarding the fabric of this city and can provide a basis for the derivation of related thermophysical properties. The data provided accurate and fine-resolution distribution of various surface types and land covers at a resolution of 30 cm. The makeup of Sacramento, based on flight data mapped onto USGS LULC 11 through 17 is summarized in Table 2.

Table 2: Sacramento Surface Makeup (%) Based on Flight Data and Mapped Onto USGS LULCs 11 Through 17

<i>LULC</i>	<i>Tree Cover</i>	<i>Roof</i>	<i>Road</i>	<i>Sidewalk</i>	<i>Parking</i>	<i>Barren</i>	<i>Grass</i>	<i>Misc.</i>
11	14.7	19.3	12.7	8.0	4.8	10.2	24.5	5.6
12	9.5	19.8	15.5	3.7	31.0	7.25	9.3	3.8
13	8.1	23.4	7.3	1.3	20.0	19.7	6.0	14.3
14	0.0	5.0	80.0	1.0	10.0	4.0	0.0	0.0
15	2.8	19.2	10.3	1.3	32.1	15.6	5.6	13.1
16	26.8	23.7	17.6	4.5	9.5	2.1	7.1	8.7
17	26.8	23.7	17.6	4.5	9.5	2.1	7.1	8.7

Assuming appropriate thermophysical properties for each surface cover in the top row of Table 2, at a resolution of 30 cm, resulted in more accurate estimates of USGS 200-m-averaged properties than the assumptions used in generating the corresponding entries in Table 1. These assumed physical properties are summarized in Table 3:

Table 3: Assumed Properties for 30-cm Resolution Land Covers

<i>Surface</i>	α	Z_0	η	ρ	k	c	Qf	f
Tree	0.163	350	0.2	1.4	0.0057	0.35	0	1
Roof	0.2	35	0	1.6	0.0033	0.3	10	0
Road	0.14	5	0	1.6	0.0033	0.3	40	0
Sidewalk	0.14	5	0	1.6	0.0033	0.3	0	0
Parking	0.14	5	0	1.6	0.0033	0.3	10	0
Barren	0.18	5	0.05	1.6	0.005	0.3	0	0.05
Grass	0.18	12	0.3	1.8	0.0038	0.44	0	1
Misc.	0.157	51.4	0.05	1.6	0.0033	0.3	18.6	0.08

The result of transposing the entries in Tables 2 and 3 is an updated properties input for categories 11-17 in the meteorological model and simulations. The updated properties are shown in Table 4.

Table 4: Updated Thermophysical Properties of Urban Land-Uses (Categories 11-17)

<i>LULC</i>	α	Z_0	η	ρ	k	c	Qf	f
11	0.170	65.90	0.111	1.62	0.0039	0.342	8.54	0.40
12	0.161	56.19	0.088	1.61	0.0039	0.332	9.56	0.19
13	0.169	42.29	0.081	1.62	0.0038	0.330	10.05	0.16
14	u	u	u	u	u	u	u	u
15	0.163	118.15	0.101	1.56	0.0042	0.332	8.54	0.102
16	0.163	55.76	0.056	1.59	0.0037	0.319	10.20	0.347
17	u	u	u	u	u	u	u	u

In this table, “u” indicates unchanged from corresponding entry in Table 1. This is unchanged because no corresponding category (or associated data) were identified in the Sacramento orthophotos.

Table 4 replaces the top (corresponding) portion of Table 1 in our simulations and was used as such throughout this study. The modified properties given in this updated portion of the table, although based on Sacramento data, were also used in developing input for simulating the other two regions in this study (until data for these regions become available). The rest of Table 1 (categories 21 through 92) were used as they are, unchanged. An effort is currently underway to analyze similar data from Salt Lake City, Baton Rouge, and Chicago to determine the degree to which the urban fabric of U.S. cities can be accurately characterized based on a variety of factors.

Finally, the distribution of USGS LULC was determined for each grid cell in the modeling domain. Values for all characteristics for each grid cell were assigned and averaged over final grid resolution for input to the meteorological model. All parameters were averaged as in equation 1 except for roughness length, which, due to nonlinearity, was averaged as in equation 2.

$$P = 1/A \sum P_i A_i \quad (1)$$

$$Z_0 = \Pi (Z_{oi})^{A_i/A} \quad (2)$$

Here, P_i is the value of a parameter in sub-area A_i , Z_{oi} is the roughness length of LULC (i) whose area is A_i . An approach similar to that in equation (2) has been used by other researchers as well (e.g., Vihma and Savijarvi 1991).

Averaging with equations (1) and (2) is reasonable in the context of this study since the mesoscale model does not explicitly treat sub-grid-scale variability in surface properties or meteorological conditions. Explicit treatment of canopy-layer dynamics is not yet a feasible feature in mesoscale models, although efforts are underway in that direction (e.g., Mestayer and Bornstein 1998, Taha 1999, Taha and Bornstein 1999). To-date sub-grid-scale variability in surface properties is accounted for mostly through this type of averaging in model input.

In the following sections, we discuss the gridded surface properties derived and used as input to the base-case mesoscale meteorological simulations of each of the three regions in this pilot project.

Salt Lake City

Figure SLC-1 depicts the topographical (elevation) data for the SLC modeling domain. The resolution is 2 km and the domain contains 9657 surface grid cells. Elevation ranges from the Salt Lake surface level (at 1265 m above MSL) in the northwestern part of the domain (left area of the figure) to the highest elevations on the eastern mountain ranges (right of figure) which reaches up to 3197 m above MSL (north points to the upper left corner of the page). The figure highlights the complex topography in the Salt Lake City region, which is a factor in the meteorology and air quality conditions in the area. Such complex topography can have a significant effect on generating terrain-induced flow as well as dispersion and trapping of air pollutants.

Figures SLC-2 through SLC-9 show the SLC domain 2-km gridded albedo, vegetative fraction, density, thermal diffusivity, surface wetness, roughness length, specific heat, and anthropogenic heat flux, respectively. As mentioned earlier in this report, these gridded values were generated based on our assumptions in conjunction with using the USGS LULC data (see Tables 1 through 4) and our aerial orthophotos data (from Sacramento).

Based on these assumptions and calculations, albedo in the SLC region domain ranges from a low of 0.05 for water (Salt Lake) to up to 0.45 in small areas with abundant exposed rocks, sand, or salt flats. These values correspond reasonably well to our independent observations and measurements of various surface and land-cover types. The high-albedo areas can be seen to the southwest of the Salt Lake as well as at the western boundary of the domain. The urbanized areas in the domain appear to have an albedo in

the range of 0.14 to 0.18. Most of the domain has an albedo in this range, which is in agreement with our past modeling and observational studies (e.g., Taha 1997, Sailor 1993).

Vegetative fraction ranges from a low of close to zero in urban areas and areas closer to the lake to a high of 0.55-0.6 east of the lake and on the southern and eastern elevations and forests. Vegetative fraction in the vicinity of SLC is on the order of 0.15 to 0.20. Overall, only 20% of the domain has vegetative fraction greater than 0.40.

The spatial distribution of parameters such as thermal diffusivity, density, surface moisture availability, roughness length, and specific heat, follows very closely the type of land cover in the area. Examining the corresponding figures, one can clearly identify the Salt Lake area as well as another smaller lake to the southeast. Aside from these two water bodies, the distribution of thermophysical properties follows the distribution of vegetated and barren lands in the area.

Soil moisture availability appears to be fairly low in the SLC domain. Our calculations suggest that the average land-surface moisture availability is about 0.12. The distribution of roughness length varies significantly across the domain. Aside from the main water bodies and flats, roughness length's distribution responds to variations in ground cover in the region (from urban, to forest, to high mountains).

Anthropogenic heat flux distribution clearly follows the distribution of urbanized areas and major highways in the region. This type of heat flux cannot be measured directly; rather, it is derived from other indicators such as energy use. The maximum man-made heat flux is modulated with a Fourier series to obtain hourly flux profiles (Taha 1998) as explained in section 1.B.3 of this report. The largest anthropogenic heat flux is found near Salt Lake City and to the north (Ogden) where it reaches around 20 W m^{-2} .

Baton Rouge

Figure BR-1 shows the topography of the Baton Rouge modeling domain. The resolution of the data is 2 km and the domain consists of 4700 surface grid cells. Elevation change in this domain is relatively small ranging from MSL at the Gulf to ~ 90 m above MSL to the north. Thus the BR domain is essentially flat and there is no complex or peculiar topography in the region, compared to that of SLC, for example.

Figures BR-2 through BR-9 show the BR domain 2-km gridded albedo, vegetative fraction, density, thermal diffusivity, surface wetness, roughness length, specific heat, and anthropogenic heat flux, respectively. Again, these gridded values were generated based on our assumptions in conjunction with using the USGS LULC data (see Tables 1 through 4) and our aerial orthophotos data (from Sacramento), as mentioned earlier in describing the SLC domain.

Albedo is seen to range from a low of 0.06 over water (Lakes Maurepas and Pontchartrain in the southeast, the Mississippi and the swamps) to up to 0.18 (with the

exception for a small areas with an albedo of up to 0.2). This contrasts sharply with the SLC domain albedo (which ranged up to 0.45 in desert areas). Large swamps appear in near-yellow regions in the figure and the Mississippi River shows very clearly as a north-south running stream. The reason for relatively lower albedo in the Baton Rouge domain is the abundance of vegetative cover, marshes, and wet lands. The BR metro area is undistinguishable and its albedo is no different from that of surrounding areas. The urban and surrounding albedo is in the range of 0.16 to 0.17.

Vegetation cover ranges from a low of 0.2-0.3 at the swamps surrounding the lakes, the swamps to the southwest of the domain, and around the Mississippi riverbed to a high of 0.6 in about one fourth of the land area in the domain. Urban BR appears to have a vegetative cover in the range 0.2 to 0.25. In general, the region is heavily vegetated and, in contrast with the SLC domain, over 65% of the Baton Rouge domain has a vegetative cover greater 0.40.

Because the region is more uniform (no topographical or major land-cover changes) the spatial distribution of parameters such as thermal diffusivity, density, surface moisture availability, roughness length, and specific heat is relatively more uniform than in the SLC domain. Surface moisture availability is relatively high and uniform in this domain, except for lower values at urban BR on the order of 0.1. Most of the domain has surface wetness in the range of 0.3 to 0.5. The distribution of roughness length seems to vary significantly across the domain. Aside from the main water bodies (the two lakes), roughness length's distribution appears to follow vegetation cover.

Anthropogenic heat flux distribution follows the distribution of urbanized areas and major highways in the region. As explained earlier, the figure shows the spatial distribution of the maximum man-made heat flux value, which is later modulated through a Fourier series to obtain hourly flux profiles. The largest anthropogenic heat flux is found in the northern tip of Baton Rouge, where it reaches around 20 W m^{-2} . Along the major communication arteries, it reaches up to about 5 W m^{-2} .

Sacramento

Figure SAC-1 shows the gridded topography for the Sacramento modeling domain. There are 1118 surface grid cells in this domain with a resolution of 4 km. The figure shows significant elevation changes and some topographical features to the east. The Central Valley floor (foreground in figure) is at about sea level (although a few spots are actually lower than MSL). The eastern ranges (Sierra) in the domain reach up to 2736 m above MSL and have an influence on the regional meteorology and dispersion of pollutants.

Figures SAC-2 through SAC-9 show the base-case gridded albedo, vegetation fraction, thermal diffusivity, density, surface wetness, roughness length, specific heat, and anthropogenic heat flux, respectively. As in the SLC and BR cases, these gridded values were generated based on our assumptions of thermophysical parameter values along with USGS LULC and orthophotos data. The resolution in these figures (and data) is 2 km.

Albedo in the SAC modeling domain is rather uniform since most of the area is agricultural with the exception of Sacramento's vicinity, surrounding and remote urban areas, and major water bodies. Albedo ranges from a low of 0.08 in a few spots (such as lakes and the San Francisco Bay in the southwestern portion of the domain) to up to 0.22 in one particular grid cell. However, the overwhelming area of the domain has an albedo around 0.18 and the urban area has an albedo of 0.14-0.16.

Vegetation fraction in this domain is relatively high. Over 80% of the domain has vegetative fraction higher than 0.40, mainly due to prevalence of agricultural areas and forests. The urban zones appear to have vegetation cover in the range 0.10-0.20. The spatial distribution of other parameters such as density, surface moisture availability, specific heat, and roughness, follows very closely the type of land cover in particular the cropped/agricultural areas versus urbanized or barren lands.

Anthropogenic heat flux reaches up to 19 W m^{-2} in urbanized areas. Along major highways, it is approximately 8 W m^{-2} . The maximum heat flux values are modified later to obtain hourly flux profiles, as discussed in section 1.B.3 this report. Table 5 summarizes some aspects of the previous discussion.

Table 5: Some aspects of the modeling domains.

<i>Region</i>	<i>Domain elevation range (m)</i>	<i>Domain albedo range</i>	<i>Urban albedo range</i>	<i>Domain vegetation range</i>	<i>Urban vegetation range</i>	<i>Domain area with vegetation > 0.4</i>	<i>Domain soil moisture average</i>
SLC	1265-3197	0.05-0.45	0.14-0.18	0-0.55	0.15-0.20	20%	0.12
BR	0-90	0.06-0.18	0.16-0.17	0-0.60	0.20-0.25	65%	0.40
SAC	0-2736	0.08-0.22	0.14-0.16	0-0.60	0.10-0.20	80%	0.25

Surface Change Scenarios

The basis for developing IAIV surface change scenarios (increased albedo and increased vegetative fraction) is the USGS LULC and the aerial photography data described earlier. For each surface type, a certain level of albedo increase was assumed based on our laboratory and field measurements (e.g., Berdahl and Bretz, 1997). The assumptions we make for increasing albedo per surface type are (for the scenarios modeled in this study and reported here): increase in residential roof albedo by 0.3, commercial roof albedo by 0.4, roads by 0.25, sidewalks by 0.2, and parking lots by 0.25. This is a final number for each surface type, i.e., after accounting for weathering and soiling effects on initial increase in albedo. Taha et al. (1992) and Pomerantz et al. (1999) discuss albedo measurements and values for a wide range of urban surface types. Pomerantz et al. (1999) also discuss the change in albedo over time, i.e., the effects of weathering and aging.

For vegetative cover modifications, the assumption we make is that each building unit in USGS LULC categories 11, 12, 15, 16, 17 gets an additional 4 trees (in the scenarios simulated and reported here), and each unit in LULC category 13 gets an additional 6 trees. It is assumed that each tree, upon maturity, will cover a top-view area of 50 m^2 .

The USGS LULC category 14 (transportation) does not get any additional trees. Also, no albedo or vegetative cover changes are assumed for categories 21 through 92. Table 6 summarizes the resulting changes in albedo ($\Delta\alpha$) and vegetative cover (Δf).

The total area considered for albedo modification (area “seen” by the meteorological model) is reduced to reflect the effect of increased canopy cover, e.g., trees covering roads, parking lots, and other built-up surfaces. In the scenarios described in this report, only one level of changes in surface properties, that is, only one IAIV scenario (for each region) was simulated (based on Table 6). Any other scenario could be simulated following the same methodology.

Table 6: IAIV Scenarios Assumptions for Modeling Sacramento, Baton Rouge, and Salt Lake City Regions

<i>USGS LULC (Urban Land Use ID)</i>	<i>$\Delta\alpha$ (200-m grid)</i>	<i>Δf (200-m grid)</i>
Residential (11)	+0.118	+18% of cell area
Commercial (12)	+0.175	+18% of cell area
Industrial (13)	+0.145	+8% of cell area
Transportation (14)	+0.237	+4% of cell area
Industrial/Commercial (15)	+0.162	+12% of cell area
Mixed Urban (16)	+0.136	+11% of cell area
Mixed/Built-up (17)	+0.155	+11% of cell area

This scenario represents a feasible *upper bound* for potential modifications in each land use category. Based on the land-use analysis performed in this study, it does not appear reasonable to increase albedo or vegetative fraction by larger amounts.

The changes given in Table 6 are on a 200-m grid-cell basis. These changes are then averaged to the meteorological model's grid size (between 2 and 4 km) a hundred times or more, depending on the grid interval selected for simulation. Thus, the final increases in albedo and vegetative fraction in the models' grids are generally smaller than given in Table 6. Table 7 summarizes the changes as they pertain to the meteorological modeling domains and grids of each region.

**Table 7. Albedo and Vegetative fraction Changes Statistics
(in meteorological modeling domains)**

	SLC	BR	SAC
Total cells in domain (including water)	9657 (x4 km ²)	4700 (x4 km ²)	1118 (x16 km²)
Number of modified cells (over entire domain)	868	1876	480
Largest albedo increase (in any one cell, anywhere in domain)	0.20	0.21	0.14
Representative albedo increase in urban core area	0.13	0.11	0.13
Largest vegetation fraction increase (in any one cell, anywhere in domain)	0.18	0.18	0.17
Representative vegetation cover increase in urban core area	0.16	0.14	0.14

In the rest of this section, we briefly discuss the modifications as they pertain to each modeling domain after the increases shown in Tables 6 and 7 are “implemented.”

Figures SLC-10 and SLC-11 show the spatial distribution of increases in albedo and vegetative cover in the Salt Lake City domain. The largest increases in albedo and vegetation fraction are seen around the SLC core as well as along the major freeways. The urban SLC core is clearly visible to the right of the figures’ center, as well as other “satellite” urban areas, such as around Ogden in the north, Orem-Provo in the southeast, and Tooele in the west. These are areas with largest increases in albedo and vegetation fraction.

Figures BR-10 and BR-11 depict the spatial distribution of the increases in albedo and vegetative cover in the Baton Rouge domain. The largest increases in albedo and vegetation fraction are seen in the Baton Rouge region (roughly at the center of the figure) and the area around Hammond to the east. The main communication routes are clearly visible in Figure BR-10 because some of the albedo increases occur along them in flanking urbanized cells.

Finally, Figures SAC-10 and SAC-11 show spatial distributions of increased albedo and vegetative cover for Sacramento. The largest increases in albedo and vegetation fraction are seen in the Sacramento metropolitan area and surrounding satellite areas, such as Davis, Stockton, and Vallejo. Again, some of the main communication routes are clearly visible these figures as surface modifications occur along them.

1.B.3 INITIAL AND BOUNDARY CONDITIONS

The meteorological simulations were performed for the base case as well as several modified scenarios for each region. Results from these simulations were used as boundary conditions input to photochemical models (directly) and to emission processors

(indirectly) to adjust the emissions of various precursors to changes in meteorological conditions.

Initial Conditions

A set of initial values for meteorological variables was used to begin the simulations for each region. The variables include temperature, dew point, pressure, wind direction, wind speed, solar radiation, cloud cover, and rain/snow. NOAA archival soundings data for 1200Z (UTC) were used, corresponding to 0400 in Sacramento, 0500 in Salt Lake City, and 0600 in Baton Rouge.

Where the vertical levels of the model and the soundings do not coincide, data for model heights were interpolated from those at pressure levels of the soundings. This was accomplished through simple linear interpolation. All interpolated variables, except atmospheric moisture, were used directly as input to the model. Dew-point data from the soundings was translated to specific humidity for input to the model using standard moist-air thermodynamic relationships, e.g.:

$$\mu = \epsilon e / (p - (1 - \epsilon) e) \quad (3)$$

where the vapor pressure e (in mb) is computed from the Magnus equation as:

$$e = 6.11 \times 10^{a\tau / (b + \tau)} \quad (4)$$

where τ is dew point temperature ($^{\circ}\text{C}$), p is pressure in mb, and for $T_{\text{air}} > 0^{\circ}\text{C}$, $a = 7.567$, and $b=239.7$ (here, $\epsilon = 0.622$). For the modified scenario (IAIV), the same initial conditions of the base case were used.

Lateral Boundary Conditions

The lateral boundary conditions for prognostic meteorological variables are set to continuity, i.e., zero gradient at the boundaries. Because of this restriction, the modeling domain is selected to be large enough such that the boundaries are far removed from the analysis sub-domain. The same boundary conditions are used for case IAIV. Modified boundary conditions should be interesting to investigate because, at least in theory, if upwind urban areas (e.g., outside of modeling domains) adopt IAIV strategies, then the boundary conditions should be modified accordingly to somehow account for this effects. But this was not done in this study.

Top Boundary Conditions

In our simulations, the model is set up such that the top boundary conditions are those of an absorbing layer spanning the uppermost 4 levels of the domain. This type of boundary conditions (Newtonian cooling and frictional dissipation of velocity) prevents vertically-propagating disturbances from being reflected back down into the domain.

Lower Boundary Conditions

The lower boundary conditions are specified through the solution of the surface energy balance equation. For land surfaces in the domain, the parameters specified in Tables 1 and 4 are used in the computation of the surface energy balance. In addition, we modified the energy balance at the first level of the model (2.5 m AGL for scalar variables) to include anthropogenic heat flux from motor vehicles, buildings, and power plant operations as a heat source term. To do so, each LULC is assigned a maximum value of anthropogenic heat flux (as in Tables 1 and 4), and this value is modified using a Fourier series to obtain the hourly profile at each grid cell. According to Sailor (1993) and Taha (1998), the series is:

$$F(t) = \gamma + \sum_n \{ \lambda_n \cos (2n\pi t/24) + \phi_n \sin (2n\pi t/24) \} \quad (5)$$

Where $n=1,3$ and $\gamma=0.557$, $\lambda_1= -0.227$, $\lambda_2= -0.006$, $\lambda_3= -0.084$, $\phi_1= -0.384$, $\phi_2=0.016$, and $\phi_3= -0.012$.

Over water bodies, the lower boundary conditions are those of constant water-surface temperature (which we specify based on SST climatologies), and are time-independent during the simulated episode. This latter assumption is reasonable since water is well mixed and its surface temperature does not change over a span of a few days (modeling episodes). For SLC, the Salt Lake water surface is kept at 286K (55.4°F), for the Lakes of Maurepas and Pontchartrain south east of BR, the temperature is kept at 290K (62.6°F), and so is that of the San Francisco Bay water.

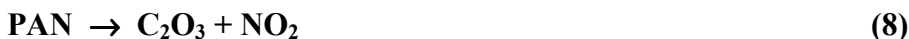
1.C Photochemical Modeling

1.C.1 MODELS AND DATA

The photochemical (air quality) simulations in this study were performed using various versions of the Urban Airshed Model (UAM) as appropriate to each region. The UAM is a three-dimensional, Eulerian, photochemical model capable of treating both inert and chemically-reactive atmospheric pollutants. It simulates the advection, diffusion, transformation, emission, and deposition of pollutants. It treats about 30 chemical species and uses the carbon bond CB-IV mechanism (Gery et al. 1988). The UAM accounts for emissions from area and point sources, elevated stacks, mobile and stationary sources, and vegetation (biogenic emissions). Version 6.20 of UAM-IV has been recommended by the US EPA for ozone air quality modeling studies of urban area.

The photochemical modeling in this study was performed using a more standard version of UAM-IV for Salt Lake City and Baton Rouge and a special version of UAM-IV for Sacramento. That version, 5.52, differs from the regulatory UAM-IV in that it directly imports the four-dimensional distribution of temperature, winds, and humidity from the meteorological model. Another difference between the two versions of relevance to the strategies of interest (i.e., temperature decrease from IAIV) is that of PAN chemistry,

thought to be most influential in ozone formation through the production of nitrogen dioxide. In the UAM, related reactions are:



The rate constants and temperature dependence factors for these reactions are different in different UAM versions. The implication of these differences is that the PAN chemistry and, thus, ozone production, is slightly more sensitive to temperature in the standard version than it is in version 5.52. However, the resulting implications are not large (Emery et al. 1997). Overall, the use of the standard version may result in less accurate estimates of the effects of IAIV strategies.

Emission and meteorological data for airshed modeling were obtained from the air-quality control agencies in each state/city participating in the UHIPP. The emission inventories were obtained as UAM-ready input, e.g., time- and space-dependent emissions from area and point sources, elevated stacks, biogenic sources, and motor vehicles. UAM meteorological input (temperature, diffusion break, humidity, and wind fields) was also obtained from the states and cities. In practice, the emission inventories can be recreated, in part or as a whole, using meteorological conditions obtained from a meteorological model (e.g., CSUMM), in conjunction with known emission-rate factors and information on level of activity at various emission sources. One advantage of this method, though involved, is the tight coupling between the simulated meteorological fields and emission rates of pollutants as well as their concentrations in the atmosphere. This procedure also allows for regeneration of the emission inventories for any scenario with modified meteorology.

Historically, however, air quality regulators and officials have preferred to use their own emission inventories and meteorological data in air quality studies. This is an appreciated fact as these data have been developed and/or evaluated by the respective agencies and, accordingly, deemed most appropriate for use in modeling. For this reason, we did not attempt to regenerate the inventories or meteorological input to the UAM in simulating the base-case scenarios. Where questionable data were encountered, we did not attempt at correcting them or generating substitutes.

Consequently, the photochemical base-case scenario for each region in this study was established using as much as possible input data (UAM meteorology and emissions) obtained from the local air quality regulatory agencies. The modified photochemical scenarios (corresponding to heat island mitigation) were simulated using modified UAM input obtained by mapping the corresponding meteorological and emission changes onto the input to UAM, as will be explained in Section 1.C.2.

Based on our earlier modeling studies, we estimate that NO_x emissions are reduced by about 1% (of their gridded hourly values) as a result of heat island mitigation. This reduction is applied to each modeling region and all NO_x sources. To estimate the changes in biogenic VOC emissions, e.g., isoprene, an environmental correction algorithm that accounts for temperature, humidity, solar radiation, and CO₂ concentrations, was used (Guenther et al. 1993). Isoprene emissions are sensitive to temperature changes. In the regions studied here, the changes in isoprene emissions are on the order of 3-10% of their hourly gridded values. As with the meteorological fields, the modifications to NO_x and VOC emissions were carried out with the mapping procedure described in the next section without having to resort to emission pre-processors that are typically used in the modeling community.

1.C.2 APPROACH

The photochemical base-case scenario for each region in this study was established using most of the UAM input data obtained from the air-quality control agencies in each state/city participating in the UHIPP. The modified photochemical scenarios (corresponding to modified surface conditions) were simulated using modified UAM input obtained by applying a four-dimensional mapping procedure (discussed below) to each respective base-case input parameter to the UAM.

Emission Inventories

The emissions inventories were obtained as UAM-ready input, e.g., time- and space-dependent emissions from area and point sources, elevated stacks, biogenic sources, and motor vehicles.

Air Quality Initial and Boundary Conditions.

For each region and episode, the air quality simulations were initialized with observational/diagnostic data obtained from the states and local air quality regulatory agencies. Similarly, the boundary conditions were specified according to data provided by these sources.

Four-Dimensional Mapping

A procedure was developed in this modeling exercise to map four-dimensional difference arrays ($\Delta = \Delta(x,y,z,t)$) of meteorology and emissions onto base-case UAM input to generate the modified scenario input. This mapping procedure is used as a more direct tool compared to available meteorology and emissions processors typically used in air quality modeling. In those cases, both base and IAIV input would need to be processed and thus all input to UAM would be generated in this study. But since we wanted to use as much as possible the states' own input data, this mapping procedure was developed so that *changes* in meteorology and emissions could be mapped.

The mapping is done on the meteorological variables (temperature, humidity, winds, and mixing heights) and emission rates of ozone precursors (biogenic and anthropogenic emissions). Dynamic consistency in the meteorological parameters is ensured to a certain extent when using fields produced by the meteorological model. Of course, this approach inherently assumes that the original input to the UAM (that is the UAM-ready input obtained from the cities) is itself dynamically consistent, which may or may not be the case.

Temperature

Mapping of the temperature onto the UAM-ready temperature input was done simply by:

$$T'_{\text{uam}}(\mathbf{x},\mathbf{y},\mathbf{z},\mathbf{t}) = T_{\text{uam}}(\mathbf{x},\mathbf{y},\mathbf{z},\mathbf{t}) + \Delta T_{\text{CSUMM}}(\mathbf{x},\mathbf{y},\mathbf{z},\mathbf{t}) \quad (9)$$

where T' and T are the new and original UAM temperatures and ΔT is the change in temperature corresponding to the IAIV scenario simulated in this study. The mapping of temperature is quite straightforward.

Mixing height

The change in mixing height, or diffusion break in UAM terms, is simply mapped as:

$$Zi'_{\text{uam}}(\mathbf{x},\mathbf{y},\mathbf{t}) = Zi_{\text{uam}}(\mathbf{x},\mathbf{y},\mathbf{t}) \times RZi_{\text{CSUMM}}(\mathbf{x},\mathbf{y},\mathbf{t}) \quad (10)$$

where RZi is the CSUMM-simulated ratio of IAIV-to-base mixing heights.

Problems related to mapping of mixing height include: 1) possible errors in CSUMM's modeling of mixing height and 2) the relatively simplified handling of diffusion break in UAM. As a result, the change in mixing height and its mapping onto UAM-ready diffusion break input can import errors. Given that the simulated pollutant concentrations, including those of ozone, are sensitive to changes in the diffusion break, these errors in mixing height estimates (base-case or modified case) can be problematic.

Wind

The mapping of the u- and v-components of the wind velocity vector is done with:

$$U'_{\text{uam}}(\mathbf{x},\mathbf{y},\mathbf{z},\mathbf{t}) = U_{\text{uam}}(\mathbf{x},\mathbf{y},\mathbf{z},\mathbf{t}) \times RU_{\text{CSUMM}}(\mathbf{x},\mathbf{y},\mathbf{z},\mathbf{t}) \quad (11)$$

$$V'_{\text{uam}}(\mathbf{x},\mathbf{y},\mathbf{z},\mathbf{t}) = V_{\text{uam}}(\mathbf{x},\mathbf{y},\mathbf{z},\mathbf{t}) \times RV_{\text{CSUMM}}(\mathbf{x},\mathbf{y},\mathbf{z},\mathbf{t}) \quad (12)$$

where Ru and Rv are the ratios of CSUMM-simulated IAIV-to-base wind speeds. Generally, the changes in wind velocity corresponding to case IAIV is relatively small, in the order of less than 1 m s^{-1} (2.2 mph) and are often negligible.

Specific Humidity

Modification of specific humidity (only for version UAM-IV 5.52) is done in a manner similar to the mapping of wind or mixing height, i.e., percentage-wise. But the changes are generally small and often negligible.

Anthropogenic Precursor Emissions

Previous modeling studies, e.g., Taha (1996,1997), Taha et al. (1998), and Haney and Fieber (1994) indicated that changes in anthropogenic emissions of ozone precursors as a result of IAIV strategies are very minimal, on the order of ~1%. With numbers of this magnitude, it is not justifiable to perform detailed and time-consuming pre-processing of emissions from point, area, and mobile sources for photochemical modeling. Instead, the present study uses a “hard-wired” reduction of 1% in NO_x and VOC emissions from the above sources.

Biogenic VOC Emissions

Unlike anthropogenic emissions, our past modeling efforts suggest (Taha 1996,1997) that changes in biogenic VOC emissions (BVOC) resulting from IAIV strategies are significant and should be accounted for properly in the simulations. This can include both increases and decreases in emissions following changes in air temperature and other meteorological parameters. The BVOC emissions in question are those from vegetation *already* in place, not new vegetation “added” in IAIV strategies. The latter are assumed to be non-polluting, zero emitting species. In this study, the mapping of changes in BVOC (isoprene and monoterpenes) resulting from changes in meteorology is done using an environmental correction algorithm (Guenther et al. 1993). As with the meteorological fields, the modifications to emissions in this study were done within the mapping procedure without having to resort to emission inventories or emission pre-processors.

In this mapping, we compute the changes in isoprene emissions, representing some 80% of all BVOC emissions, and ignore changes in monoterpenes. Thus, for each grid cell and hour, the modified isoprene emissions are computed from:

$$E_{IAIV} = E_b + \left. \frac{\partial E^*}{\partial T_a} \right|_{T_a} \cdot \Delta T_a \quad (13)$$

where E_{IAIV} and E_b are the isoprene emission rates for the modified (IAIV) and base-case (b) conditions, respectively, the partial derivative represents the slope of the correction relationship at current air temperature (T_a), and ΔT_a is the change in air temperature at a certain time and grid cell resulting from IAIV. Note that this (and other equations) are three dimensional, but the indices (x,y,t) were dropped for simplicity.

Here,

$$E^* = \left\{ e^{c1[T-Ts]/RTTs} \right\} / \left\{ 1 + e^{c2 [T-Tm]/RTTs} \right\} \quad (14)$$

where c_1 , c_2 , T_s , and T_m are constants, R is the gas constant, and T is air temperature.

Mapping Changes in Initial and Boundary Conditions

Following the same logic, it would be straightforward to map changes in initial concentrations of pollutants and space- and time-dependent changes in boundary conditions for concentrations. However, such modifications were not performed in this study because it was assumed that the IAIV scenarios were locally implemented in a region of interest and that the surrounding (e.g., upwind) regions did not implement these strategies. Also, initial conditions (concentrations) were not changed because the objective in this case is to test the efficacy of the IAIV strategies in modifying the base conditions while the upwind conditions have not changed. Otherwise, one could have initialized the UAM simulations using cleaner-air conditions (initial and boundary conditions and emissions).

Modeling Domains and Episodes

Table 8 describes the CSUMM and UAM modeling domains for each of the three regions.

Table 8. Modeling domains and grids.

1	2	3	4	5	6
	Grid spacing	E-W grids	N-S grids	Vertical levels and model top	Domain area (km ²)
CSUMM					
SLC	2x2 km	87 (172 km)	111 (220 km)	22 (9 km)	37840
BR	2x2 km	94 (186 km)	66 (130 km)	22 (9 km)	24180
SAC	4x4 km	43 (168 km)	34 (132 km)	22 (9 km)	22176
UAM					
SLC	4x4 km	44 (172 km)	56 (220 km)	5 (2.0 km)	37840
BR	2x2 km	66 (130 km)	66 (130 km)	5 (1.8 km)	16900
SAC	4x4 km	40 (156 km)	34 (132 km)	5 (1.5 km)	20592

The modeling episodes (meteorological and air quality) in this study were selected to match the air quality modeling episodes used by the states/cities in SIP modeling work. For Salt Lake City, the episode is August 11-12 (1996), for Baton Rouge it is May 24 and 25 (1990), and for Sacramento, it is July 11 through 13 (1990).

2. Modeling Results

2.A Meteorological Modeling Results

OVERVIEW

In this section, results from mesoscale meteorological modeling are discussed for each simulated region (SLC, BR, SAC). The discussion will focus on three meteorological variables of relevance to air quality modeling: 1) air temperature, 2) wind field, and 3) mixing height. The temperature and wind fields are presented at the first level of the model, i.e., 5 m for wind and 2.5 m for temperature, because this is where most of the changes in meteorology occur as a result of surface modifications. Past similar modeling efforts, e.g., Taha (1996,1997), showed that the bulk of the changes in meteorology occurs near the surface and that some changes do occur higher above the ground, their magnitudes being smaller than those near the surface.

All meteorological results are discussed in this section for the last day of the multi-day simulated episode in each region. This is done to avoid model spin-up errors and contamination of results with initial conditions. The last day we discuss for each region typically corresponds to the third (or fourth) day of the meteorological modeling episode. To keep the discussion compact, results from a few hours from the last day are shown and discussed.

Salt Lake City

Base Case Conditions

The meteorological simulations for SLC show that the effect of topography (imparting a chaotic pattern on temperature distribution) is quite significant. The higher elevations have a consistently lower temperature than the lower elevations (for example compare the temperature distributions in Figure SLC-12 with the topography shown in Figure SLC-13). In the figures, the city itself (SLC) is in the area defined by easting coordinates grids: $52 < X < 60$ and northing coordinates grids: $53 < Y < 62$, which is slightly to the right of the figure's center. Immediately to the east of urban SLC, terrain elevation results in significant drop in temperatures.

In terms of urban air temperatures and heat island (UHI), the simulations suggest that the urban area is generally warmer than its immediate surroundings. The UHI appears to be on the order of up to 4K (7.2°F) at night and early in the morning but up to 2K (3.6°F) during the afternoon hours. Averaged over urban areas, the nighttime UHI is about 2K (3.6°F) and that of daytime is 1K (1.8°F). However, the aerial extent of the UHI is larger in the afternoon than earlier during the day. In absolute terms, the urban-SLC air temperature is in the range of 295-297K (71.6-75.2°F) in the morning and in the range of 303-305K (86-89.6°F) in the afternoon.

Note that the definition and reporting of UHI depends on a reference, non-urban location's temperature. This can be ambiguous in locations with complex topography and mixed land-surface types such as the Salt Lake City region. Therefore, while the selection of a reference, rural station for UHI assessment may be somewhat arbitrary, the “rural” location selected for SLC in this report is such that it is at the same elevation as that of the urban area and that it is not too far from it, yet not affected by its heat plume. For the SLC modeling domain, the area selected to represent “rural” conditions, or non-urban, is located about 15 km due west of Salt Lake City.

Air temperature over the lake is not uniform due to air masses being advected from different land and water areas (see convergence zone in Figure SLC-13) but is generally lower than the urban air temperature during most of the diurnal cycle. Depending on wind flow, there may be hotter or colder air over the lake. The simulated wind field suggests that during the night and early morning hours, local topographical/terrain effects are dominant, e.g., downslope flow. While the downslope flows are evident, they tend to have a more westerly tendency. The flow over the Lake suggests an eddy or generally turning flow at the western end of the lake. In addition, both simulations and observations show an easterly wind tendency in the flow over the lake. At 0600 LST, the maximum wind speed is 8.7 m s^{-1} (19 mph) occurring over the Salt Lake.

During the afternoon hours, e.g., 1400 and 1600 LST (Figure SLC-13, for example), the flow is mostly from the south over most of the domain. Over some portions of the central domain and over the lake, there is a west component to the wind. Obviously, the large-scale flow is more dominant at this time than the terrain-induced flow, although the latter can still be seen around hills and higher elevations in the figures. The wind field was qualitatively compared to data from Salt Lake City's Utah Office of Air Quality and was found to be comparable and reasonable. Although some northerly displacement of eddies was noticed, the general flow and reversal patterns were reasonably comparable to observational data. Also, the simulated wind speed agrees with observed speeds with the maximum being on the order of 6 m s^{-1} (13 mph).

In terms of mixing height, the simulations suggest a noisy signal, as expected in a region of significant terrain changes (and also in part because the model does not do well in simulating mixing heights). The main phenomenon to look for is the characteristic rise of the boundary layer during daytime and its fall back at night. Another feature is the low mixing height over the lake and increased height over rough terrain due to increased mixing, e.g., Figure 14. Earlier in the morning, e.g., at 0600, for example, the domain-averaged mixing height (averaged over 9657 cells) is 109 m and at 1600 LST, it is 1669 m.

While discussing these aspects of the base-case meteorology, one should recall that these fields (in absolute terms) will not be used in the air quality modeling. Only *differences* between the base-case and those of IAIV cases will be used, as explained earlier in the section on four-dimensional mapping.

Modified Scenario

The simulations suggest that the urban areas (as well as other areas closer to the lake) are generally cooler than in the base-case. At night, urban areas that were modified with case IAIV run about 0.5-1.5K (0.9-2.7°F) cooler than in the base-case, although there are some spots where temperature actually increased by up to 1K (1.8°F). However, the vast majority of the domain (not affected by case IAIV) is unchanged.

During daytime, which is of most interest to this study's objectives, the areas affected by IAIV strategies, e.g., urban SLC, are about 1.5-2K (2.7-3.6°F) cooler than in the base-case conditions. The largest cooling is seen to happen at SLC proper (e.g., Figures SLC-15) and along the SLC-Ogden “corridor”. The other cooling (blue areas) are associated with other urbanized cells that were also modified with IAIV strategies. See again Figures SLC-10 and SLC-11 that show the distribution of increased albedo and vegetative fraction. The simulations suggest that IAIV strategies more than offset the heat island effect at periods of higher absolute temperatures, i.e., after 1200 LST (see Table 9 for a summary). In the modified scenarios, temperature can increase in some locations due to a change in the wind flow pattern and stability/mixing in areas of wind pattern change, especially downwind of urban areas. The changes in wind are due to changes in the temperature gradients and/or increased roughness following implementation of IAIV strategies.

As an example, Figure SLC-16 depicts the wind flow pattern associated with case IAIV for Salt Lake City. In general, the simulations suggest no detectable difference in wind field from the corresponding times in the base-case scenario. There are some very minor differences in the flow over the lake at 1400 and 1600 LST. In general, the wind flow (both direction and magnitude) is not affected by IAIV strategies, and the largest difference in the wind speed between the two cases anywhere in the modeling domain is less than 1 m s^{-1} (2.2 mph).

The mixing in case IAIV height is generally lower than that in the base case. However, there are also slight increases in the mixing height elsewhere in the domain. In the affected cells, the change is smaller than $\pm 10\%$ of the base-case gridded values at corresponding times. Figure SLC-17 shows an example snapshot of the simulated mixing height corresponding to case IAIV.

Baton Rouge

Base Case Conditions

Compared to the SLC results, the simulated temperature field for BR is more uniform, especially during daytime, e.g., Figure BR-12, due to lack of significant changes in elevation and terrain features. The air temperature above the lakes is either equal to or lower than over the land, at all hours. In this figure, the city of Baton Rouge is located in

the area defined by easting coordinates grids: $40 < X < 50$ and northing coordinates grids: $20 < Y < 27$, which is about at the center of the figure and slightly to the left.

The simulations suggest that the urban area is generally warmer than its immediate surroundings, especially at night. Compared to the Salt Lake City heat island, the simulated Baton Rouge UHI is relatively larger and better defined at night than during the daytime. At 0200 LST, for example, the Baton Rouge UHI appears to be on the order of 2-4K (3.6-7.2°F). At 0500, the UHI is smaller and almost vanishes at 0600 LST with an intensity of about 1K (1.8°F). As mentioned in the SLC discussion, the definition and reporting of UHI depends on a reference, non-urban location's temperature. And while this was somewhat problematic for SLC due to topography, it is relatively easier in Baton Rouge since the area is flat and more uniform. However, there were different gradients to the east and the west of BR proper making it necessary to use more than one reference point to get a fair evaluation of the UHI.

During the daytime, the UHI in Baton Rouge is smaller, e.g., about 0.5K (0.9°F) at 1400 and 0.5-1K (0.9-1.8°F) at 1600 LST. In absolute terms, the urban-BR air temperature is in the range of 293-295 (68-71.6°F) early in the morning and in the range of 306-307K (91.4-93.2°F) in the afternoon.

The simulations suggest a uniform wind field over most of the domain except for the areas near the two lakes in the south east and the marshes to the south west, where the wind direction changes significantly. The simulated flow is generally southerly at night and early during the morning with the highest winds in the southern portion of the domain. At 0600, for example, the maximum wind speed is 4.2 m s^{-1} (9.2 mph). During the day, the flow over the lakes is still south-to-north with a stronger component in this direction due to the “lake breeze” effect. The rest of the domain, however, has a northerly flow in general at 1400 and a easterly flow at 1600 LST (see Figure BR-13 for example). At 1600 LST, the maximum wind speed is 5.7 m s^{-1} (12.5 mph). As mentioned earlier, the absolute wind velocities are not used in the air quality simulations, only changes in the wind field.

Compared to the noisy signal in SLC (due to complex topography) the mixing height field is relatively smoother over the Baton Rouge domain (see Figure BR-14 for example). During the night and early morning hours, the mixing height is in the vicinity of 100-150 m, extending to at most about 0.5 km at some locations. During the most unstable part of the day, it can reach up to about 2 km, further inland, but is still low over and near the lakes. Over urban BR, there is a slightly more elevated boundary layer than the immediate surroundings, as a result of increased mixing. In terms of domain-averaged mixing height (averaged over 4700 cells), the 0600 average height is 125 m and the 1600 height is 1362 m.

Modified Scenario.

The simulations of case IAIV for BR suggest that the urban areas at night and early morning hours can be warmer or cooler than their surroundings. During these hours,

urban areas can be up to 2K (3.6°F) cooler and up to 1.5K (2.7°F) warmer than the surrounding areas. Significant changes also occur near the northern edge of the lakes due to changes in the wind field in that area. During the daytime, urban areas are about 0.5-1K (0.9-1.8°F) cooler than the surrounding areas. For example, compare Figure BR-15 to the change in albedo in Figure BR-10.

Over the entire domain, some areas can be up to 2-3K (3.6-5.4°F) cooler at night and during the daytime. The warming, overall, can reach the same range, especially at the north edge of the lakes, where the changes in wind are largest between the base-case and IAIV scenarios. The simulations suggest that IAIV strategies more than offset the heat island effect at periods of higher absolute temperatures, i.e., after 1200 LST. But both UHI and IAIV impacts are small, e.g., in the order of 1K (1.8°F); see Table 9 for a summary. Because the region has relatively high soil moisture content (lakes, marshes, bogs) evapotranspiration from increased vegetative cover in the area is smaller than in drier regions. As a result, this mechanism does not contribute much to cooling the air and most of the decrease in temperature in this region is a result of increased surface albedo.

Compared to the base-case conditions, the wind field corresponding to case IAIV is not significantly different, but there are some changes at certain locations, e.g., near the lakes. At 0200 LST, for example, the wind flow in the southern portion of the domain has a slightly stronger northerly component. Due to the change in winds at these locations at 0200 LST, the temperature difference is positive, i.e., increased temperature in the IAIV scenario. At 0500 LST, most of the changes happen north of the lakes where a subsidence cell forms and results in heating. Roughly the same changes happen at 0600 LST. It is to be noted, however, that aside from the slight change in direction, speed changes are smaller than 1 m s^{-1} (2.2 mph).

During the daytime (see Figure BR-16, for example), the southerly component of the wind is smaller in case IAIV, meaning weaker flow near the gulf and the lakes due to smaller surface temperature gradient as a result of IAIV “implementation”.

Finally, the mixing height corresponding to case IAIV is generally lower than that in the base case, although there are also areas with increased mixing height. In the affected cells, the change is smaller than $\pm 8\%$ during the day and at night. During the day, the relatively elevated boundary layer over urban areas in the base case becomes lower and undistinguishable from that of the surrounds (e.g., Figure BR-17). Because the region is very uniform and almost homogeneous, the changes in the mixing height are very smooth and credible (compared to the case of SLC).

Sacramento

Base Case Conditions

As with SLC, the simulations of Sacramento suggest a significant impact from topography. The eastern half of the domain is consistently cooler (higher elevations of the Sierra foothills), whereas the western half has some variations following land-cover and

water distributions. At 0200 LST, there is a UHI of 3K (5.4°F). The simulations also suggest that areas with relatively lower vegetative cover, e.g., a north-south “strip” in the middle of the domain, also have higher temperatures (see the figure, for example). After 1200 LST, the pattern of temperature distribution becomes a strong function of elevation. Sacramento itself experiences a 0.5-1K (0.9-1.8°F) heat island at this hour and through 1700. In terms of absolute temperature, urban Sacramento is approximately 300-303K (80.6-86°F) at night and early morning, and in the neighborhood of 311K (100.4°F) between 1400 and 1600 LST. See Figure SAC-12 for example.

Figure SAC-13 shows a snapshot of the simulated wind vector field at the lowest layer of the model, overlaid on topography (colored background). The simulated wind field was compared to observational data from the California Air Resources Board (CARB) and found in general to be consistent, although local-scale differences exist. During the night and early morning hours, the downslope flow is dominant in the eastern portion of the domain. The model also produces an eddy in the southwestern portion of the domain during these hours. At 0600, the maximum wind speed is 3.9 m s^{-1} (8.5 mph) occurring just to the northeast of Sacramento metro and in the foothills. During the afternoon hours, e.g., 1400 and 1600 LST, the flow is mostly from the west (sea breeze from the San Francisco Bay) and topographically-induced flow is not dominant. At 1600, the maximum wind speed is 5.6 m s^{-1} (12.3 mph).

In general, the simulated mixing height field is uniform and smooth, except for some perturbations in the eastern domain, where the Sierra foothills are, as well as to the west of the domain where the SF Bay area hills are located (see Figure SAC-14 for example). At night and early morning, e.g., 0200, the mixing height on the average is approximately 100 m. The maximum PBL height at that hour is ~1200 m on the western elevations. At sunrise, e.g., 0600 LST, the mixing height is still about 200 m on the average, but with a maximum now of about 1400 m. After that time, the PBL increases in thickness very rapidly as it becomes unstable. For example, at 1600, the average mixing height is approximately 1000 m and the maximum is at 3500 m near the NE corner of the domain (in the Sierra). The domain-averaged (1118 cells) mixing height at 0600 is 73 m and at 1600 LST it is 1217 m.

Again, in discussing all these aspects of the base-case meteorology, it is important to keep in mind that the absolute terms of these fields will not be used in the air quality modeling. Only *differences* between the base-case and IAIV cases (in terms of meteorological fields and mixing height) will be used, as explained elsewhere in this report. That is, changes in temperature, winds, moisture, and mixing height, not their absolute values, will be mapped onto UAM-ready input in simulating the air quality conditions for IAIV strategies in each region.

Modified Scenario

The simulations suggest that during the night, the difference in temperature (from the base case) is chaotic due to lateral mixing, eddies circulations, and other factors. Thus it is difficult to generalize the nighttime results. During the daytime, however, the IAIV

strategies have a more consistent and predictable effect. At 1400 LST, the Sacramento metro area is cooled by up to 1.6K (2.9°F), and by up to 1.2K (2.2°F) at 1600 LST (e.g., Figure SAC-15). However, compared to SLC and BR the area affected by temperature decrease is larger in Sacramento. For example, the area affected by a change of at least –1K (-1.8°F) is about 1200 km². In BR and SLC, the corresponding area is about 200-400 km². This explains in part why IAIV measures in Sacramento result in a greater improvement in air quality than in SLC or BR, as will be discussed later. Thus even though the maximum cooling is slightly larger in SLC, the affected area is smaller than in Sacramento and thus the effect on air quality, as we will see later, is smaller. The simulations suggest that IAIV more than offset the local UHI in Sacramento during the afternoon hours. See Table 9 for a summary.

In terms of wind field changes, the simulations suggest that during night- and early-morning hours, there is some effect on the wind field in the western (flat) part of the domain. Areas of convergence are slightly displaced and new ones are created. There is not much change in the wind field over the foothills, but mostly around metropolitan Sacramento. Here again, the size of the area modified with IAIV seems to have a larger impact (than in SLC and BR) on the wind field. During the afternoon hours, most of the IAIV effect is again found in the western part of the domain. In this case, the wind flow is stronger towards the east (area of lower temperatures) than in the base-case conditions where there is meandering of the wind to the north or south. The effect of IAIV on the daytime/afternoon wind flow pattern is to strengthen the San Francisco Bay's sea-breeze effect and add a more westerly component to the flow. At night, again, the front of the reverse flow (land breeze) is slightly delayed; the position of the front is moved further to the north and northeast in case IAIV compared to the base case. But in general, the changes in wind speed itself are smaller than 1 m s⁻¹ (2.2 mph). See Figure SAC-16, for example.

Finally, the mixing height is generally lower than that in the base case. In the affected cells, the change can be up to ± 10% of the base-case gridded values, e.g., Figure SAC-17.

SUMMARY OF METEOROLOGICAL MODELING RESULTS

The mesoscale simulations suggest that the three regions modeled in this study do have heat islands and that these heat islands are larger at night than during the daytime. The modeling work also suggests that the implementation of IAIV strategies *more than offsets* the local urban heat island in each region, especially during the afternoon. Table 9 provides a summary of temperature-related findings for urban areas in each of the three regions. The areas used in computing these attributes do not include all modified or urban areas in the domain, only areas deemed representative of the changes in each of the three cities. For this table, the area considered in the calculations are as follows: SLC: 280 km², BR: 360 km², and SAC: 2112 km².

Table 9. Summary of *Urban Air Temperature and Modifications.*
< > Indicates Most Representative Urban Temperature Attributes
at the Given Hour. Entries are in K (with °F in parenthesis).

1	2	3	4	5	6
		0200 LST	0600 LST	1400 LST	1600 LST
SLC	Base case <T>	295 (71.6 °F)	293 (68.0 °F)	303 (86.0 °F)	305 (89.6 °F)
	<UHI>	2 (3.6 °F)	2 (3.6 °F)	1 (1.8 °F)	1 (1.8 °F)
	Δ <T> (IAIV)	-1 (-1.8 °F)	-1 (-1.8 °F)	-1.5 (-2.7 °F)	-2 (-3.6 °F)
BR	Base case <T>	295 (71.6 °F)	293 (68.0 °F)	306 (91.4 °F)	307 (93.2 °F)
	<UHI>	3 (5.4 °F)	1 (1.8 °F)	0.5 (0.9 °F)	0.5 (0.9 °F)
	Δ <T> (IAIV)	-1 (-1.8 °F)	0	-0.75 (-1.4 °F)	-0.75 (-1.4 °F)
SAC	Base case <T>	3030 (86.0 °F)	300 (80.6 °F)	312 (102.2 °F)	311 (100.4 °F)
	<UHI>	3 (5.4 °F)	3 (5.4 °F)	0.7 (1.3 °F)	0.5 (0.9 °F)
	Δ <T> (IAIV)	-1 (-1.8 °F)	-1 (-1.8 °F)	-1.6 (-2.9 °F)	-1.2 (-2.2 °F)

In terms of mixing height, the simulations suggest a noisy response to IAIV strategies, as discussed earlier. However, domain-averaged values, as shown in Table 10, may be easier to remember.

Table 10. Domain-Averaged Mixing Height and Changes.

	Base (m)		IAIV (m)	
	0600	1600	0600	1600
SLC	109	1669	107 (1.8% ↓)	1664 (0.3% ↓)
BR	125	1362	114 (8.8% ↓)	1224 (10.0% ↓)
SAC	73	1217	73 (0.0% ↓)	1200 (1.4% ↓)

The simulations also suggest that the impacts on the wind field are such that there is some slowing down near the surface and some changes in direction. The changes in speed and/or direction are caused by reduced temperature gradients and increase surface roughness resulting from “implementing” IAIV strategies. Table 11 provides a snapshot of these changes.

**Table 11. Some Aspects of the Simulated Wind Field.
U- and V- Components and Changes are in m/s.**

LST	Base <u>	IAIV <u>	Δ <u>	Base <v>	IAIV <v>	Δ <v>
SLC (area=280 km²)						
0400	-1.8	-1.7	0.11	0.5	0.4	-0.05
0800	-1.9	-1.9	-0.05	-0.2	-0.2	-0.00
1200	1.0	0.9	-0.1	0.7	0.5	-0.25
1600	2.1	1.3	-0.82	3.4	2.1	-1.38
2000	-0.1	-0.1	-0.02	1.2	1.1	-0.13
2400	-1.7	-1.9	-0.14	0.1	0.4	0.41
BR (area=360 km²)						
0400	-0.4	-0.1	0.29	0.6	0.7	0.06
0800	-0.1	-0.7	-0.62	0.0	0.0	-0.01
1200	-0.0	-0.2	-0.23	-0.2	0.6	0.84
1600	-1.5	-1.8	-0.27	-1.4	-0.4	1.01
2000	-0.1	-0.7	0.24	0.6	0.3	-0.30
2400	-0.2	-0.5	-0.32	0.3	0.5	0.17
SAC (area=2112 km²)						
0400	-0.5	-0.5	-0.00	0.0	0.1	0.07
0800	-0.4	-0.4	-0.06	0.2	0.2	0.01
1200	0.5	0.2	-0.29	1.7	2.2	0.50
1600	2.4	2.0	-0.37	0.1	0.6	0.52
2000	0.8	0.3	-0.52	-0.9	-0.3	0.62
2400	-0.9	-1.4	-0.46	-0.2	0.2	0.41

2.B Air Quality Modeling Results

OVERVIEW

As a result of surface modifications (i.e., IAIV), various changes in meteorology, e.g., temperature, winds, and mixing height, occur. In general, reduced air temperatures lead to lower ozone concentrations but the simulations suggest both increases and decreases and air temperature, as discussed earlier. The most important mechanism through which air temperature affects ozone production is believed to be the chemistry of peroxyacetyl nitrate, PAN (Cardelino and Chameides 1990). In sensitivity simulations of the Los Angeles Basin, Taha and co-workers showed that decreasing an airshed's temperature *only* always results in decreasing ozone concentrations. For example, an average decrease of 12% in ozone can result when domain-wide average temperature is decreased by 1.5K (2.7°F). However, temperature changes are not the only resulting meteorological modifications from IAIV. When temperatures are lower, the depth of the mixed layer can be relatively smaller, since buoyant production of TKE (turbulent kinetic energy) is smaller. This can potentially increase local ozone concentrations or increase ozone scavenging at other times, i.e., when NO is not completely titrated. Thus there are non-

linear interactions and the net, final effects must be carefully quantified and analyzed through comprehensive meteorological and photochemical modeling. In this section, results from photochemical modeling are discussed for each simulated region (SLC, BR, SAC).

Salt Lake City

Base Case Conditions

Of the primary pollutants, the NO_x and isoprene emissions are briefly discussed here because these emissions are modified in the IAIV scenarios. Figures SLC-18 and SLC-19 show the base-case emissions of NO_x (NO+NO₂) in the SLC region for 1400 and 1600 LST on the last day of the modeling episode. It is apparent that these emissions are mostly confined to the major north-south urbanized corridor. As expected, the largest emissions are in the SLC core (seen at the center of the figure), reaching to some 562 g.mole per hour (per km²). Figures SLC-20 and SLC-21 show the 1400 and 1600 LST emissions of isoprene in the region. These emissions are mostly from the vegetated slopes and forests. There, these emissions can peak up to about 25 g.mole per hour (per km²). Isoprene emissions increase with temperature and solar radiation and these numbers are for the times of the peak. The urban areas, e.g., north-south corridor, on the other hand, seem to be devoid of any significant isoprene emissions (less than 2.5 g.mole/hr per km² emissions of isoprene) due to lack of or small vegetative cover.

Figure SLC-22 shows the base-case ozone concentrations, as simulated with the UAM for the episode of August 11-12 (1996) for the peak hour, e.g., 1700 LST. This is the simulated ozone concentration at the lowest layer of the UAM for the second day of the photochemical modeling episode. The simulations show that the highest concentrations are found to the west, south, and, in particular, to northwest of urban SLC. Concentrations close to and over the lake are generally higher than over urban SLC. The UAM simulations show that the peak concentration (anywhere in the domain) on August 12 is about 118 ppb northwest of the SLC core.

The simulations suggest that overall, the region peaks between 1600 and 1900 LST. With respect to the existing National Ambient Air Quality Standard (NAAQS) of 120 ppb for ozone, the region is in attainment during this (simulated) episode although concentrations reach the neighborhood of 120 ppb northwest of SLC during one or two hours. With respect to the possible revised NAAQS for ozone of 80 ppb, however, there are violations in many locations in this domain. These UAM simulations generally underestimate the observed concentrations during that episode. Aside from potential errors in data and models mechanisms, the lower urban ozone concentrations can be attributed to titration by NO in areas where it is emitted in larger amounts.

Modified Scenario

In terms of precursor emission changes resulting from the impacts of IAIV strategies (temperature effects), Figures SLC-23 and SLC-24 depict the estimated decrease in NO_x emissions (NO+NO₂) from the base case. Of course the changes (-1%) follow the same north-south corridor of NO_x emissions discussed in Figures SLC-18 and SLC-19. The largest decreases are in central SLC and amount to about 4.4 g.mole/hr (per km²). Figures SLC-25 and SLC-26 depict the changes (increases or decreases) in isoprene emissions as a result of IAIV strategies. These were computed based on the environmental correction algorithm described earlier in this report. Note that the changes are very insignificant and scattered. There are small increases in emissions where temperature increased and vice versa (temperature increases in some areas due to changes in stability/wind field as the temperature gradients change following IAIV strategies). The changes do not affect the urban areas and “corridor” where there are few emissions of isoprene in the first place. Most of the changes in emissions happen over the higher elevations and the forests. The aerial extent of increases and decreases seems to be equal and within the range of ± 0.4 g.mole/hr (per km²).

We now discuss some aspects of the changes in ozone concentrations as a result of IAIV strategies. The changes we discuss here include the effects of changes in meteorology as well as changes in emissions resulting from IAIV strategies. Later in this section, we will discuss the resulting effects from meteorological changes only, without modifications in emissions of precursors.

Overall, IAIV strategies have a modest impact on improving the air quality in the Salt Lake City region. A typical decrease of 3-4 ppb in urban areas between 1400 and 1600 LST is about 3% if it were compared to the urban peak (~95 ppb), and a reduction of 2.5% if compared to the domain peak (~118 ppb) at these hours. Compared to other regions, e.g., Baton Rouge and Sacramento, as well as previous modeling results, e.g., Los Angeles (Taha 1996,1997), the SLC decreases in ozone of 2.5-3% are relatively small. The primary explanation for this is likely due to the smaller/limited area of IAIV modifications, which is mostly confined by topography to narrow freeway-following urban areas, not large or contiguous like in other regions.

The simulations suggest that by 0700 LST, the urban areas can experience a decrease of up to 4 ppb in ozone concentrations, whereas other areas in the domain can see increases of 1 or 2 ppb. But these areas are less extensive than the ones with decreased concentrations.

In Figure SLC-27 for example, a difference in ozone concentrations (from the base case) is shown for a peak hour. It is clear that the vast majority of the domain is unchanged in terms of ozone concentrations, but that there are significant areas with decreased ozone of about 3-4 ppb. At 1200 and 1400 LST, the decrease in ozone concentrations is up to 3 ppb in areas northwest of the SLC core. In the SLC core itself, the decrease is about 2 ppb. At 1600 LST, the magnitude of the decrease is still about 3 ppb, but the area affected by the decreased concentrations is much larger than earlier during the day. Also, at 1600,

there are now areas with noticeable increases in concentrations. The increase is also on the order of 1-3 ppb but the area affected by increased concentrations is smaller than the region affected by decreased concentrations. Also, the increases seem to occur in non-urbanized zones. At 1400 LST, the ratio of the number of grid cells with decreased concentrations to the number of cells with increased concentrations is 1.87 domain wide (from this point forward, this ratio will be referred to as the “D/I ratio”). Note that this is not the most useful way of portraying changes in ozone because it does not account for population distributions. The best method would be to perform population-weighted exceedance exposure assessment but was not performed due to unavailability of *gridded* population distribution data at the time of this writing. The same argument applies for BR and SAC and will not be repeated there.

The simulations suggest no changes in the domain or urban peaks for ozone. The changes in ozone concentrations in SLC seem to be small compared to other regions previously modeled, e.g., Los Angeles (Taha 1996,1997). The reasons for this include: 1) smaller areas available for modifications (for IAIV strategies), and 2) different approach for surface modification calculations. In addition, the location of the peak is not coincident with urban areas (that is, areas where surface modifications are assumed). Thus while there is a benefit where surface modifications occur, the remote location where the peak is does not see any impact.

To understand whether the changes in ozone (as a result of IAIV) are caused mostly by meteorological changes or by changes in meteorology-dependent emissions (i.e., temperature-dependent emissions), a test UAM run was performed to include only meteorological changes (corresponding to IAIV case) while keeping emissions of precursors at the base-case level. The results suggest no differences between the two cases (that is case IAIV with only meteorology changes and case IAIV with both meteorology and emission changes) in terms of largest increase or decrease in ozone concentrations. Otherwise stated, the effect of emissions changes (from IAIV) bears no impacts on the level of ozone concentrations changes. The spatial distributions of the concentration changes are also similar between the two cases except for minor differences in the spatial extent of the changes. At 1600 LST, for example, domain-wide statistics show that with meteorological changes *only*, the D/I ratio is 2.29. In the case where both meteorology *and* emissions were changed, the D/I ratio is 2.27, which is not significantly different from the case of meteorology only. Thus in SLC, all the changes in ozone concentrations resulting from IAIV strategies are caused by changes in meteorology. Changes in emissions have no impact because they are small and, in case of BVOC, remote.

Baton Rouge

Base Case Conditions

Figures BR-18 through BR-21 depict the base-case emissions of NO_x (defined as NO+NO₂) and isoprene in the Baton Rouge (BR) modeling domain. As before, these figures show emissions at the hours of 1400 and 1600 LST. The emissions of NO_x are

concentrated in the urban core area where they reach up to about 190 g.mole/hr (per km²). While the emissions of NO_x are focused near the urban core, the isoprene emissions cover the entire land portion of the domain, because the area is heavily vegetated. The highest emissions are found at the northwestern portion of the domain as well as to the east of BR. In these areas, emissions can reach up to about 38 g.mole/hr (per km²). In urban BR and along the urbanized corridor stretching to the south, emissions of isoprene are low, close to 2.5 g.mole/hr (per km²) or less.

Figure BR-22 shows the base-case ozone concentrations at peak time for the Baton Rouge region on the last day of the May 24-25, 1990 episode. These are concentrations at the lowest layer of the UAM for the second day of the episode. Urban BR is in the middle of the figure. The simulations suggest a domain peak in the neighborhood of 153 ppb and an urban peak of about 113 ppb. The simulations show that overall, the region peaks between 1300 and 1500 LST. During this period, concentrations exceed the existing NAAQS for ozone (120 ppb) in many areas of the region.

Modified Scenario

Figures BR-23 and BR-24 show the assumed reductions in NO_x emissions as a result of IAIV strategies. These can be reduced by up to about 1.8 g.mole/hr (per km²) in the core areas. In addition, Figures BR-25 and BR-26 show the changes in isoprene emissions corresponding to these strategies. As mentioned earlier, these changes are computed with an environmental correction algorithm described earlier in this report. As expected, the changes in NO_x emissions occur in the core area only, whereas the changes in isoprene emissions are more sporadic, following to some extent the distribution of vegetation and changes in air temperature resulting from case IAIV. Most changes in isoprene do not occur in the urbanized areas, but rather in the heavily vegetated surrounding area. The changes range from about -4 to +1 g.mole/hr (per km²) and are almost negligible.

We now discuss some aspects of the air quality impacts of IAIV strategies. In general, the simulations suggest that the benefits of IAIV occur mostly during the first half of the day. In the afternoon, the effects are smaller. Figure BR-27, for example, shows some aspects of the changes in ozone concentrations as a result of IAIV (this is not the time of the peak but the time of some of the largest decreases in ozone resulting from IAIV). These changes include the effects of meteorology as well as changes in emissions resulting from IAIV strategies (later in this section, we discuss the resulting effects from meteorological changes only, without modifications in emissions of precursors). The simulations suggest that the decreases in concentrations can reach up to 5 ppb in the urbanized areas (at 0900), whereas the increases, generally smaller in extent, can reach up to 2 ppb in remote areas of the domain. By 1000 LST, both increases and decreases reach 4 ppb, but the area with decreased concentrations is larger than that with increased ozone.

IAIV strategies have a slightly larger impact on air quality in BR compared to that in SLC in terms of largest decrease in concentrations reached at any time. However, most of the effect and its spatial dominance happen before noontime. A decrease of 5 to 6 ppb in

urban areas in the BR domain is about 5.3% of the urban peak (113 ppb), and a reduction of 3.6% if it were compared to the domain peak (153 ppb). Note that these are not time- or location-coincident concentrations and changes.

The largest changes in ozone are seen around central BR and along the urbanized corridors of the cities of St. Gabriel, Carville, Geismar, Prairieville, and Gonzales. This is seen as a band stretching from the center of the domain and towards west-south-east. At 1000 LST, the effect is similar in spatial distribution (see Figure BR-27) and magnitude, albeit smaller in extent than earlier in the morning. By noontime, only central BR and some portions of the corridor enjoy decreased concentrations. Other areas see increased ozone. After noontime, the effects of IAIV are smaller. For example, the change in concentration at 1500 LST is only on the order of 1 ppb and, later, no benefits from IAIV are seen.

Thus unlike SLC, IAIV in BR causes reductions in peak concentrations (albeit small) and domain-averaged concentrations. This is in addition to decreasing concentrations by up to 6 ppb in urban areas which is slightly better than in SLC.

While some areas in the domain see minor increased concentrations as a result of IAIV strategies, most see a decrease in ozone concentrations. During the first half of the day, the areas with decreased concentrations are dominant (at least 5 times larger than those areas with increased concentrations) and the net effect is a decrease in ozone concentrations. For example, at 1000 LST, the D/I ratio is 2.32, whereas at 1200 LST, the D/I ratio is 1.74.

As was done with SLC, we tested whether the changes in ozone in BR are caused mostly by meteorological changes or changes in temperature-dependent emissions. For this purpose, a test UAM run was performed to include only meteorological changes (from case IAIV), keeping emissions of precursors at the base-case level. Unlike the case with SLC, the simulations suggest that there is some difference between a case with both meteorology and emissions changes and a case with only meteorological changes as far as they affect the resulting simulated ozone concentrations in Baton Rouge. The difference, however, is not in the magnitude of the change (e.g., maximum change) but in the spatial extent of the changes. In the case with meteorology only, the total area affected by the decreased concentrations is smaller than in the case where both meteorology and changes in emissions are taken into consideration. The difference in area is on the order of 4-6%. For example, at 1000 LST, the D/I ratio for the case with meteorology only is 2.00 (instead of 2.32). At 1200 LST, the case with meteorology only has a D/I ratio of 1.35 (instead of 1.73). Thus the effects of changes in emissions resulting from IAIV contributes towards improving the air quality in the region by increasing the area of decreased concentrations (increasing the area by 5-6%) and decreasing the area of increased concentrations (decreasing the area by 8-9%). These numbers are for the entire modeling domain. Changes in emissions have a relatively larger effect in BR than in SLC because, for example, isoprene emission changes occur throughout the land portion of the domain, whereas in SLC, only the higher elevations are affected and are farther from the urban areas where IAIV strategies are implemented.

Sacramento

Base Case Conditions

Figures SAC-18 and SAC-19 show the base-case emissions of NO_x (NO+NO₂) in the Sacramento region for 1400 and 1600 LST on the last day of the modeling episode. The largest emissions are concentrated in the Sacramento metropolitan area (slightly to the right of the figure's center), reaching up to some 412 g.mole per hour (per km²). It can also be observed (especially in Figure SAC-19) that these NO_x emissions follow the main highways in the region (heading northeast of Sacramento towards Auburn and Placerville and to the southwest, towards Davis, Fairfield, and Vallejo). Figures SAC-20 and SAC-21 show the 1400 and 1600 LST emissions of isoprene in the region. The figures show some unusual spatial distribution with emissions concentrated in a few areas near the boundaries of the domain (but were used as such in this modeling study). The highest concentrations are found to the east of Sacramento, peaking to about 188 g.mole/hr (per km²). As mentioned earlier, isoprene emissions increase with temperature and solar radiation and these numbers are for the times of the peak. The urban areas, on the other hand, seem to have low emissions of isoprene due to small vegetative cover. Most of the domain seems to have emissions less than 25 g.mole/hr (per km²).

We now present some aspects of the base-case air quality conditions in Sacramento, as simulated with the UAM for the July 11-13 (1990) episode. The SMAQMD and the CARB have prepared their modeling episode's data for use in version 5.52 of UAM. Accordingly, this version was used in simulating Sacramento in this study. The simulations suggest that the highest concentrations are generally found to the northeast of Sacramento's core. This is the area between Sacramento and the city of Auburn (see Figure SAC-22 for example).

The simulations suggest that the peak concentration (anywhere in the domain) on July 13 is in the range of 80-86 ppb at 1000 LST, 80-100 ppb at 1200, 100-120 at 1400, and finally 130-150 ppb at 1600 (during the first day of the modeled episode, concentrations reach as high as 171 ppb). Areas close to Downtown Sacramento appear to have concentrations of about 40-60, 60-80, 60-80, and 70-90, at these hours respectively. However, the area affected by these high and moderate concentrations is relatively very large. This encompasses regions near Lodi (south of domain), Davis, Sacramento, Charmichael, Roseville, Citrus heights, Placerville, and Auburn. It even extends further north east of Auburn towards the Lake Tahoe region. The domain maximum ozone on the last day of the simulated episode is 139 ppb to the north east of Sacramento.

Modified Scenario

Figures SAC-23 and SAC-24 depict the assumed decrease in NO_x emissions (NO+NO₂) from the base case. Of course the changes follow the same pattern of spatial distribution of NO_x emissions discussed earlier. The largest decreases are in central Sacramento and

along the major routes in the area reaching up to some 5 g.mole/hr (per km²). Figures SAC-25 and SLC-26 show the changes in isoprene emissions as a result of IAIV strategies. These were computed based on the environmental correction algorithm described earlier. Unlike BR and SLC, the changes in isoprene emissions computed for Sacramento are all negative (decreased emissions). The changes, however small, occur primarily in one area to the east of Sacramento where the emissions were assumed to be concentrated.

Overall, heat island mitigation strategies significantly improve air quality in SAC with reductions in ozone concentrations of 7 and 10 ppb at 1400 and 1600 LST, respectively (about 6% and 8% of the domain peak at these hours, 112 ppb and 132 ppb respectively). SAC achieves greater reduction in ozone as a result of IAIV strategies compared to SLC and BR, mainly because of its larger geographical area, which allows a cumulative temperature and emissions reduction effect. The domain peak at 1700 LST of 139 ppb is reduced to 130 ppb.

The simulations suggest no clear benefit from IAIV strategies during the early hours of the morning and up to 1000 LST, as both increases and decreases in concentrations are of the same magnitude. The benefits of IAIV begin at about 1100. At 1200 LST, the Sacramento-Auburn corridor achieves lower concentrations (a decrease of up to 5 ppb). Areas closer to the domain boundaries see increased concentrations, but only by up to 3 ppb. That effect is further amplified in the afternoon so that the corridor enjoys concentrations of up to 7 ppb lower at 1400 and 10 ppb lower at 1600 (see Figure SAC-27, for example). During these two hours, the corresponding increases in the northeastern domain portion are 4 and 4 ppb respectively. From this it is clear that the effects of IAIV in Sacramento are significant. The increases in ozone concentrations occur in non-urbanized zones and thus have no negative effects with regards to population exposure to smog. At 1400 LST, D/I ratio is 2.52 and at 1600 LST it is 3.23. In terms of domain-averaged concentrations, the simulations suggest that case IAIV lowers the domain average by about 1 ppb, or up to 2 ppb at times.

To test whether the changes in ozone are caused mostly by meteorological changes or by temperature-dependent emissions, a test UAM run was performed to include only meteorological changes (from case IAIV) but keeping emissions of precursors at the base-case level. The simulations suggest that the difference between the two cases is in the range of concentrations decreases, e.g., at 1200 LST (a difference of 1 ppb in the range of concentrations decrease). But as with the other cities, the spatial extent of the benefits or changes in concentrations is affected, too. For example at 1400 LST, the D/I ratio is 2.17 for the case with meteorology only (instead of 2.52). At 1600 LST, the D/I ratio is 2.87 in the case with meteorology only (instead of 3.23).

At the location of the domain peak of 139 ppb at 1700 (third day of episode), the concentrations drop by 9 ppb (to 130 ppb) at the same location and time. Thus in general, IAIV strategies have a significant effect in Sacramento (relative to the other two regions) on improving the air quality. A decrease of 7 and 10 ppb at 1400 and 1600 LST,

respectively, is about 6% and 8% of the domain peak at these hours (112 ppb and 132 ppb respectively) on the third day of episode.

SUMMARY OF PHOTOCHEMICAL MODELING RESULTS

This section provides a summary of the air quality simulation. Table 12 provides some information with respect to the peak concentrations on the last day of the modeling episode.

Table 12: Ozone Concentration Changes at the Location and Time of the Peak During the Last day of the Modeling Episode

1	2	3	4	5
	Time of peak on last day	Urban peak (ppb) on last day**	New peak (ppb) (at same time and location)	Change
Salt Lake City	1700	94 (118)		94 0%
Baton Rouge	1500	113 (153)		112 -0.8%
Sacramento	1700	139 (139)		130 -6.5%

**Numbers in parenthesis are domain-peaks.

The table above provides peaks on the last day of the episode; larger peaks can sometimes be simulated during the first or second days. Column 4 gives the new peak at the same time and same location as the urban peak reported in column 3. Table 13, on the other hand, provides information for other hours during the last day of the episode.

Table 13: Ozone Concentrations and Changes for the Last Day of the Modeling Episode.

1	2	3		4	
	Urban Peak (at hour) ppb	Decrease (ppb) at hour		Percent change **	
Salt Lake City	88 (1400) 94 (1600)	-3 (1400)	-2 (1600)	-3.4% (1400)	-2.1% (1600)
Baton Rouge	95 (1000) 106 (1200)	-4 (1000)	-4 (1200)	-4.2% (1000)	-3.8% (1200)
Sacramento	112 (1400) 132 (1600)	-7 (1400)	-10 (1600)	-6.2% (1400)	-7.6% (1600)

** This change is with respect to the urban peak and at the hour given in parentheses.

In this table, column 2 gives the urban ozone peak concentrations (ppb) that are representative of the urban area at *the hour given in parenthesis* on the last day of the modeling episode, whereas column 3 gives the largest decrease anywhere in the domain *at that hour* and may not occur at the same location as the peak given in column 2. Table 14 gives the largest decrease in ozone *anywhere, any time during the last day of the modeling episode*. Larger decreases can be simulated during the first or second day of the simulations. As can be seen, the largest decreases can occur at times and in areas with quite low ozone concentrations, and are therefore irrelevant in SLC and BR, but important in Sacramento.

Table 14: Largest Decrease in Ozone During the Last Day of the Episode.

<i>Region</i>	<i>Largest decrease</i>	<i>Time of largest decrease</i>	<i>Concentrations (ppb)</i>
SLC	4 ppb	0700	34 → 30
BR	5 ppb	0900	54 → 49
SAC	10 ppb	1600	121 → 111

Table 15 provides some information on the areas affected by decreases or increases in ozone following the “implementation” of IAIV strategies.

Table 15: D/I Ratio at Selected Hours

1	2	3	4
Region	D/I ratio at (hr)		D/I ratio at (hr) for meteorology only
SLC	1.87 (1400)	2.27 (1600)	2.29 (1600)
BR	2.32 (1000)	1.74 (1200)	1.35 (1200)
SAC	2.52 (1400)	3.23 (1600)	2.87 (1600)

This table gives the ratio (D/I) of the total area with decreased concentrations to the total area with increased concentrations for the hours given in parenthesis (columns 2 and 3). Thus the area benefiting from decreased concentrations of ozone is about 2 to 3 times larger than the area experiencing increased smog (effects of changed meteorology and emissions as a result of IAIV strategies). Column 4 shows the D/I ratio for a case where only IAIV meteorology is accounted for (emissions are not modified from base case as a result of IAIV strategies). A comparison of columns 3 and 4 suggests that emission changes from IAIV have no impacts on the D/I ratio in SLC, a moderate impact in BR, and a relatively significant impact in SAC.

Finally, Table 16 gives information on the concentrations changes with respect to corresponding temperature changes in each urban area.

Table 16: Temperature and Concentration Correlations for Daytime Hours (Last day of episode)

<i>Region</i>	<i>Times of largest [O3] decrease</i>	<i>Temperature change (K)</i>	<i>[O3] change (ppb)</i>	<i>Dependence ppb/K</i>
Salt Lake City	1400	-1.5 (-2.7°F)	-3	2 (1.1 ppb/°F)
	1600	-2 (-3.6°F)	-2	1 (0.6 ppb/°F)
Baton Rouge	1000	-0.9 (-1.6°F)	-4	4.4 (2.4 ppb/°F)
	1200	-1 (-1.8°F)	-4	4 (2.2 ppb/°F)
Sacramento	1400	-1.6 (-2.9°F)	-7	4.4 (2.4 ppb/°F)
	1600	-1.2 (-2.2°F)	-10	8.3 (4.6 ppb/°F)

EMISSION EQUIVALENTS OF IAIV STRATEGIES

The air quality modeling results of IAIV strategies have been presented in this report in terms of ozone concentration reductions. While such information is useful in quantifying the impacts of IAIV strategies, it does not provide a scale for the relative importance of these impacts. In other words, how do these impacts compare to those of other strategies, e.g., emission controls? What is the equivalent of IAIV strategies in terms of emission reductions?

One possible way of answering these questions is to convert the reductions in ozone concentrations resulting from IAIV strategies back into VOC and/or NO_x emission reduction equivalents. Thus, in theory at least, a more concise and quantitative interpretation can be made and an easier comparison to the effectiveness of other air-quality improvement strategies can be achieved.

For this purpose, a peak ozone-concentration isopleth plot for each region was constructed using UAM. The model was run for the full episode about 100 times for each region, changing the ratio of precursor emissions (NO_x vs VOC) at each run. Historically, these plots have been generated with EKMA, using Lagrangian models. In this study, we generate them more accurately using an Eulerian model (UAM itself) and the emission input we obtained from the states/local regulatory agencies. While many variants of these plots can be generated, in this section we present only one such, that of domain-peak concentration, which is required by the U.S. EPA for ozone attainment demonstration. We discuss this method for Sacramento only, because it is the only region where the **domain peak** is actually reduced with IAIV strategies (see Table 12, column 5). Note that other regions do achieve benefits from IAIV, but not in terms of the peak and therefore are not discussed in this section.

For Sacramento, the peak ozone concentration isopleths are shown for 1700 LST on the last day of the episode (July 13) in Figure SAC-28. One hundred UAM runs were performed for various NO_x/VOC emission reductions/control scenarios starting at (100%,100%) emissions at the upper right corner of the plot to (0%,0%) emission at the origin of the figure. The model is run for the entire three-day episode each time, and the peak concentration at 1700 LST *anywhere* in the domain on the last day of the simulation episode is plotted on the chart (note that there are many other ways to generate variants of this chart). Thus, the top right corner of the chart represents the peak of 139 ppb at 1700 on the last day of the modeling episode. Two isopleths are highlighted in the figure. One corresponds to the existing NAAQS for ozone (concentration of 120 ppb) and the other to a concentration of 130 ppb. The latter corresponds to the new peak shown in column 4 of Table 12, that is, the peak corresponding to case IAIV in Sacramento.

The plots can help visualize two aspects: 1) the efficacy of IAIV strategies in helping the region reach attainment (in terms of the peak ozone), and 2) convert impacts of IAIV into

precursor emission reduction equivalents. For the first purpose, Figure SAC-28 shows that IAIV strategies can be very effective in terms of helping the area reach attainment. That is, the area to the right of the 130-ppb isopleth is greater than 50% of the area to the right of the 120-ppb isopleth (actually almost 75%). In essence, these plots suggest that implementation of IAIV strategies can move the Sacramento area more than halfway to attainment. Of course this is with respect to the peak and this conclusion may not apply to other indexes and aspects of ozone air quality. However, the conclusion to be drawn from this is that a combination of IAIV strategies and other emission control methods can result in reaching attainment much faster than with emission control strategies alone.

For the second purpose, the 130-ppb isopleth can be used to “convert” the impacts of IAIV strategies into equivalent emission reductions. For example, the figure suggests that the impact of IAIV is equivalent to 8% reductions in VOC emissions (with VOC-only control) or to 56% NO_x emission reductions (with NO_x-only control). Of course, the second scenario is not realistic but is given as an example to clarify the use of the chart. The most realistic strategies would involve a combination of NO_x and VOC control and thus will not follow the axes, but will go from the top-right of the figure to the 130-ppb line through some angle (slant). In conclusion, these charts indicate that for Sacramento, implementation of heat island mitigation measures can reduce peak ozone concentrations significantly, and that these ozone concentrations are equivalent to VOC reductions of 8% or any combination of VOC and NO_x emission reductions that will be required to “reach” the 130-ppb isopleth.

3. Conclusion

Summary

Results from this exploratory modeling effort suggest that all three cities included in this study benefit from implementing heat island reduction strategies in their areas. The mesoscale meteorological simulations indicate that the three regions (Salt Lake City, Baton Rouge, and Sacramento) have heat islands that are larger at night than during the daytime. The simulations also suggest that the implementation of IAIV (increased albedo/increased vegetative cover) strategies can more than offset the local heat islands, especially during the afternoon. In addition to temperature, the results show impacts on the depth of the boundary layer and the wind field. For the three cities studied here, the simulations suggest that average temperature reductions of about 1-2K (1.8-3.6°F) are possible over IAIV-modified areas. Changes in the mixing height are generally bound between -10% and +3%, and changes in wind speed are smaller than 1 m s⁻¹.

In terms of ozone air quality, the simulations suggest that heat island mitigation has a beneficial effect in all three regions. Corresponding ozone reductions range from about 1 to 8 ppb/K (up to 4.6 ppb/°F). The improvements in air quality are slightly smaller in Salt Lake City than in Baton Rouge, and largest in Sacramento. The domain-peak concentrations do not change as a result of heat island mitigation in Salt Lake City and

Baton Rouge, but do so in Sacramento. The urban peak does not change in Salt Lake City, while some decrease is detected in Baton Rouge as well as a relatively significant decrease in Sacramento. Overall, all three regions benefit from heat island mitigation and decreased ozone levels at peak and other locations. It is important to note that in each region, there are both areas that benefit from heat island mitigation (reduced ozone) and areas that get worse (increased smog). However, the areas with decreased concentrations are at least twice as large as areas with increased ozone, and the magnitude of decrease in concentrations is larger than the increase. Thus the net, overall effect is always a reduction in ozone concentrations so that in general, all three areas enjoy improvements in air quality after increasing albedo and vegetative cover in urban areas. Also, the increases in ozone (in affected areas) are consistently lower than NAAQS.

As would be expected, the level of improvements in meteorology (heat island mitigation) and air quality (net decreases in ozone concentrations) depends heavily on each region's meteorology and climate, geography, scale, topography, basin morphology, proximity to water bodies, land-use patterns, precursor emission rates and mix, baseline albedo and vegetative fraction distributions, and potential for modification (increasing albedo and vegetative fraction). Based on our earlier modeling efforts, we also found that the larger the modified area the larger the net reductions in ozone concentrations. In larger areas, it is possible to lower the peak ambient temperatures by as much as 4 or 5K locally (up to 9°F) and by up to 3K (5.4°F) on the average. The associated reduction in ozone concentrations, therefore, can be larger than what has been simulated in these three cities.

Finally, an important factor to keep in mind is that these cities are unique and not necessarily representative of most major urban areas in the U.S., especially in terms of scale and geography/topography. For this reason, it is not possible to extrapolate the results from this study to other regions. In particular, Salt Lake City has complex topography and a water body in its vicinity, and Baton Rouge is in a region of high surface moisture. None of these can be easily used to represent many other areas. For this reason, careful modeling is needed for each region in the future.

The implementation of IAIV is a major undertaking that requires planning and coordination among many stakeholders. But the benefits can be large and, in our opinion, are worth studying, testing, and promoting, if found to be locally promising. The potential benefits from heat island mitigation strategies can sometimes be on the same order of magnitude as that of other major air pollution control measures such as electric cars. What is even more appealing is that heat island control provides citizens with better air quality along with the added benefit of significant savings in energy costs. The USEPA has also sponsored LBNL to perform a companion study to quantify the energy benefits of implementing heat island mitigation measures (Konopacki and Akbari 2000).

Caveats

As in any simulation study, errors in model formulations, solvers, input data, and assumptions can accrue and potentially bias or even cloud the results. This is particularly critical in cases where regulatory decisions depend on such simulation results, as may be

the case in this study. There are many potential sources of errors in a modeling study of this scope and they cannot be all addressed and discussed in this report. In this section, however, we list some concerns that are more specific to this study, and that need to be borne in mind when interpreting and using the results or planning similar studies in the future. To be realistic, one must say that the issue of modeling errors will always exist and one must be extremely careful in using and interpreting results from modeling studies like this one.

Issues with Selection of Cities

As the simulations suggest, one reason for the relatively small impacts of IAIV strategies in the three cities selected for this modeling study is that the areas available for surface modification (urban) are relatively small. In addition, these three cities may be atypical in terms of size, meteorology, topography, and surface cover. This is particularly true for SLC (topography and land-cover) and BR (high ground moisture content and water cover). Sacramento may be relatively more representative of many other urban areas in similar climates, and the simulations suggest larger benefits from IAIV in that region. We expect that our modeling of other regions, e.g., Chicago and Houston, will result in relatively larger benefits since these cities are larger in aerial extent.

Issues with The Modeling Process

To provide the most efficient use of the available data, the UAM IV and CSUMM models were used in this study. We recommend that future modeling studies be performed using more advanced models, such as the PSU/NCAR MM5 and the UAM-V or MODELS3.

Although the base-case UAM simulations were performed using most of the input data we obtained from the state/local agencies, the base-case simulation results reported in this study can differ from those reported by the states. Possible reasons include differences in models/model versions as well as possible differences in the input data.

Although a qualitative assessment of the base-case model performance was done for the mesoscale simulations, no rigorous model performance evaluation was performed in this study. The CSUMM was found in previous studies to perform relatively well, except for problems associated with mixing height computation (Taha 1996,1997). The qualitative evaluations performed in this study vs. data from SLC, BR, and SAC, suggest again a reasonable performance. Some of the results suggest improved performance compared to past modeling results, e.g., Sacramento.

Due to the nature of this sensitivity study, no data assimilation, e.g., four-dimensional data assimilation (4DDA) was used. This can significantly contribute to deviation of base-case simulated meteorological conditions from those observed during the corresponding modeling episodes. While in general the mesoscale simulation results were reasonable, the potential improvement, were 4DDA incorporated, was not tested.

A method (4-D mapping) was developed and used in this study to map changes in meteorology and emissions onto UAM input. This method inherently assumes dynamic/mass consistency in the UAM input. Whether the input to UAM is consistent and, accordingly, whether the resulting mapped modified fields are consistent is unknown.

The use of UAM for SLC and BR and version UAM-IV/5.52 for Sacramento creates a situation where direct intercomparisons among the three cities is not straightforward. At this time, no other alternative was available since the data were prepared specifically for these versions.

Model “urbanization” schemes were not used in this study. These schemes, e.g., Taha 1999, can potentially result in larger effects of surface modifications on the meteorological fields, in particular, air temperature. Thus the effects of IAIV strategies could be larger than predicted in this study if urbanized meteorological models were used.

Issues with Input Data

Some UAM input data, while not necessarily erroneous, seemed questionable, e.g., BVOC (isoprene) emission distributions, diffusion break, and temperature. Errors in these parameters can result in errors when the four-dimensional mapping is performed.

This study's main focus is on the change in meteorology and its effects on emission rates and atmospheric production of photochemical smog. Thus, the benefits of IAIV strategies, simulated in this study, are a direct result of changing the temperature-dependent emission of precursors and their reaction rates. In this context, the use of modeling systems that employ the more recent chemical mechanisms can improve the accuracy, e.g., UAM-V, MODELS3.

Despite CSUMM's limitations with the handling of the boundary-layer height, other models were not used due to limited data availability and scope. Some of these issues and problems were addressed in our other modeling studies and the work of Emery et al. (1997) at ENVIRON.

Issues with Surface Modification Scenario Assumptions

In developing the modified scenarios (IAIV), the level of surface albedo and vegetative fraction increase was based on USGS LULC and aerial data. The aerial data, however, were based solely on the flights over Sacramento, but were also used for BR and SLC. Additional urban fabric analysis of other cities may demonstrate whether this is an appropriate assumption (whether these cities have similar urban fabric).

4. References

Akbari, H., Bretz, S., Kurn, D., and Hanford, J., 1997a. "Peak power and cooling energy savings of high-albedo roofs", *Energy and Buildings — Special Issue on Urban Heat Islands and Cool Communities*, Vol. 25, No. 2, pp. 117-126.

Akbari, H., Kurn, D., Bretz, S., and Hanford, J., 1997b. "Peak power and cooling energy savings of shade trees", *Energy and Buildings — Special Issue on Urban Heat Islands and Cool Communities*, Vol. 25, No. 2, pp. 139-148.

Berdahl, P. and Bretz, S.E. 1997. "Preliminary survey of the solar reflectance of cool roofing materials", *Energy and Buildings — Special Issue on Urban Heat Islands and Cool Communities*, Vol. 25, No. 2 (1997), pp. 149-158.

Building Energy Simulation Group (BESG), "Overview of the DOE-2 Building Energy Analysis Program, Version 2.1D," Lawrence Berkeley Laboratory Report LBL-19735, Berkeley, CA, 1990.

Cardelino, C.A. and Chameides, W.L. 1990. "Natural hydrocarbons, urbanization, and urban ozone", *Journal of Geophysical Research*, Vol. 95, No. D9, pp. 13971-13979.

Chang, S.C. 1999. "Developing surface-properties input for mesoscale meteorological modeling", LBNL Draft Report, Available from Author.

Emery, C., Yarwood, G., Heiken, J., and Tran, C., 1997. "Air quality modeling evaluation of the "Cool communities" ozone control strategy. Report to the SCAQMD, ENVIRON International Corp., 101 Rowland Way, Suite 220, Novato, CA 94945.

EPA 1986. "Guideline on Air Quality Models (Revised)". U.S. Environmental Protection Agency EPA-450/2-78-027R.

Gabersek, S. and Taha, H. "Impacts of surface characteristics changes on urban heat island intensity". ICB 96, 14th International Congress of Biometeorology, September 1-8, 1996, Ljubljana, Slovenia.

Gery, M.W., Whitten, G.Z., Killus, J.P. 1988. "Development and testing of the CBM-IV for urban and regional modeling", Report EPA-600/3-88-012, U.S. EPA, Research Triangle Park, NC.

Grimmond, C.S.B. and Oke, T.R. 1999. "Heat storage in urban areas: Local-scale observations and evaluation of a simple model", *Journal of Applied Meteorology*, Vol. 38, No. 7, pp. 922-940.

Grimmond, C.S.B., H.A. Cleugh, and T.R. Oke, 1991: An objective urban heat storage model and its comparison with other schemes. *Atmos. Environ.*, 25B, 311-326.

Guenther, A., Zimmerman, P., Harley, P., Monson, R., and Fall, R. 1993. "Isoprene and monoterpene emission rate variability: Model evaluations and sensitivity analysis", *Journal of Geophysical Research*, in press.

Haney, J. and Fieber, J. 1994. Unpublished technical note, Systems Applications International, San Rafael, CA.

Kessler, R. and Douglas, S. 1992. "User's guide to the Systems Applications International Mesoscale Model", SYSAPP-92/069, Systems Applications International, San Rafael, California.

Konopacki, S. and Akbari, H. 2000. "Energy savings calculations for urban heat islands mitigation strategies in Baton Rouge, Sacramento, and Salt Lake City. LBNL Report 42890.

Mestayer, P. and Bornstein, R.D. 1998. "Workshop on the linkage of numerical urban canopy layer and PBL models". *Bulletin of the American Meteorological Society*, Accepted.

Mulberg, E. 1999. Personal Communication. California Air Resources Board, Sacramento, California.

Parker, D. and Barkaszi, S., 1997. "Roof solar reflectance and cooling energy use: Field research results from Florida", *Energy and Buildings – Special Issue on Urban Heat Islands and Cool Communities*, Vol. 25, No. 2, pp. 105-115.

Pielke, R., 1984. "Mesoscale Meteorological Modeling," Academic Press.

Pielke, R. 1974. "A three-dimensional numerical model of the sea breeze over South Florida", *Monthly Weather Review*, 102:115-139.

Pomerantz, M., Pon, B., Akbari, H., and Chang, S.C. 1999. "The effect of pavement temperatures on air temperatures in large cities", LBNL Draft report No. 43442.

Rose, S., Taha, H., and Akbari, H. 1999. "Characterizing the fabric of the urban environment: A case study of Sacramento, California". LBNL Draft Report, Available from Authors.

Sailor, D. 1993. "Role of surface characteristics in urban meteorology and air quality", Ph.D. dissertation, University of California — Berkeley.

Simpson, J. and McPherson, E.G., 1997. "The effects of roof albedo modification on cooling load of scale model residences in Tucson, Arizona", *Energy and Buildings—Special Issue on Urban Heat Islands and Cool Communities*, Vol. 25, No. 2, pp. 127-137.

Taha, H. 1999: "Modifying a Mesoscale Meteorological Model to Better Incorporate Urban Heat Storage: A Bulk-Parameterization Approach", *Journal of Applied Meteorology*, Vol. 38, pp. 466-473.

Taha, H. and Bornstein, R. 1999. "Urbanization of meteorological models and implications on simulated heat islands and air quality". Invited paper, International Conference of Biometeorology and International Conference on Urban Climatology, November 8-12, 1999, Sydney, Australia.

Taha, H., Konopacki, S., and Gaberseck, S. 1999a. "Impacts of large-scale surface modifications on meteorological conditions and energy use: A 10-region modeling study", *Theoretical and Applied Climatology*, vol. 62, no. 3-4, pp. 175-185.

Taha, H. 1997. "Modeling the Impacts of Large-Scale Albedo Changes on Ozone Air Quality in the South Coast Air Basin", *Atmospheric Environment*, Vol. 31, No. 11, pp. 1667-1676 (1997).

Taha, H. 1996. "Modeling the Impacts of Increased Urban Vegetation on the Ozone Air Quality in the South Coast Air Basin", *Atmospheric Environment*, Vol. 30, No. 20 (1996), pp. 3423-3430.

Taha, H., Sailor, D., and Akbari, H. 1992. "High-albedo materials for reducing building cooling energy use", LBNL report No. 31721 UC-350.

Vihma, T. and Savijarvi, H. 1991. "On the effective roughness length for heterogeneous terrain", *Quarterly Journal of the Royal Meteorological Society*, Vol. 117, pp. 399-407.